PCCP

Intermolecular Interactions in Clusters of Ethylammonium Nitrate and 1-Amino-1,2,3-triazole

Journal:	*Physical Chemistry Chemical Physics*
Manuscript ID	CP-ART-05-2023-002407.R1
Article Type:	Paper
Date Submitted by the Author:	13-Sep-2023
Complete List of Authors:	Kim, Shinae; Iowa State University, Chemistry Conrad, Justin; Iowa State University Tow, Garrett; University of Notre Dame, Chemical Engineering Maginn, Edward; University of Notre Dame, Chemical and Biomolecular Engineering Boatz, Jerry; Air Force Research Laboratory Aerospace Systems Directorate Edwards AFB Gordon, Mark; Iowa State University Department of Chemistry

Intermolecular Interactions in Clusters of Ethylammonium Nitrate and 1-Amino-1,2,3-triazole

Shinae Kim[1,4], Justin Conrad[1], Garrett M. Tow[2], Edward J. Maginn[2],

Jerry A. Boatz[3], and Mark S. Gordon[1]

1. Department of Chemistry and Ames Laboratory, Iowa State University, Ames, IA 50011
2. Department of Chemical & Biomolecular Engineering, University of Notre Dame, Notre Dame, Indiana 46556
3. Aerospace Systems Directorate, Air Force Research Laboratory, Edwards Air Force Base, California 93524
4. Combustion Research Facility, Sandia National Laboratories, Livermore, California 94550

Abstract

The intermolecular interaction energies, including hydrogen bonds (H-bonds), of clusters of the ionic liquid ethylammonium nitrate (EAN) and 1-amino-1,2,3-triazole (1-AT) based deep eutectic propellants (DeEP) are examined. 1-AT is introduced as a neutral hydrogen bond donor (HBD) to EAN in order to form a eutectic mixture. The effective fragment potential (EFP) is used to examine the bonding interactions in the DeEP clusters. The resolution of the Identity (RI) approximated second order Møller-Plesset perturbation theory (RI-MP2) and coupled cluster theory (RI-CCSD(T)) are used to validate the EFP results. The EFP method predicts that there are significant polarization and charge transfer effects in the EAN:1-AT complexes, along with Coulombic, dispersion and exchange repulsion interactions. The EFP interaction energies are in good agreement with the RI-MP2 and RI-CCSD(T) results.

The quasi-atomic orbital (QUAO) bonding and kinetic bond order (KBO) analyses are additionally used to develop a conceptual and semi-quantitative understanding of the H-bonding interactions as a function of the size of the system. The QUAO and KBO analyses suggest that the H-bonds in the examined clusters follow the characteristic hydrogen bonding three-center four electron interactions. The strongest H-bonding interactions between the $(EAN)_1$:$(1\text{-}AT)_n$ and $(EAN)_2$:$(1\text{-}AT)_n$ (n=1-5) complexes are observed internally within EAN; that is, between the ethylammonium cation $[EA]^+$ and the nitrate anion ($[NO_3]^-$). The weakest H-bonding interactions occur between $[NO_3]^-$ and 1-AT. Consequently, the <u>average</u> strengths of the H-bonds within a given $(EAN)_x$:$(1\text{-}AT)_n$ complex decrease as more 1-AT molecules are introduced into the EAN monomer and EAN dimer. The QUAO bonding analysis suggests that 1-AT in $(EAN)_x$:$(1\text{-}AT)_n$ can act as both a HBD and a hydrogen bond acceptor simultaneously. It is observed that two 1-AT molecules can form H-bonds to each other. Although the KBOs that correspond to H-bonding interactions in $[EA]^+$:1-AT, $[NO_3]^-$: 1-AT and between two 1-AT molecules are weaker than the H-bonds in EAN, those weak H-bond networks with 1-AT could be important to form a stable DeEP.

1. Introduction

Low melting ionic liquids (ILs) are a class of promising materials with multiple novel applications.[1,2,3,4] Generally, these ILs belong to a subset of molten ionic salts with a melting point lower than 100 ºC. Some ILs even have a melting point below room temperature, and often stay liquid under mild and ambient conditions.[5,6,7,8]

Many ILs possess a number of unique physicochemical properties including extremely low vapor pressures at ambient temperatures, high thermal stabilities, tunable viscosity, and high conductivity.[2,3,4,9] In addition, ILs can be designed to possess varied solubility in water and many organic solvents, opening up a plethora of opportunities for their use in a wide range of applications. However, some ILs suffer from drawbacks such as toxicity, difficult preparation and high cost of processing for use.[10] For example, imidazolium-based ILs show significant soil and water toxiciy.[11,12] ILs with embedded metals or halogens also require separation and purification processes for utilization and disposal.[12] Due to the aforementioned complications some ILs have the potential to become persistent pollutants - posing an environmental risk and preventing their large scale industrial manufacture and wide applicability.[11]

Deep eutectic solvents (DESs) have emerged as a new generation of solvents that can replace some ILs.[10,13,14,15] As an eutectic mixture of ionic salts and hydrogen bond donors (HBDs), DESs may exhibit similar physiochemical properties (e.g. good ionic conductivity, tunability) to ILs.[16,17] However unlike ILs, many DESs are simple to prepare and relatively low cost to produce. [16,17,18,19] Additionally they do not exhibit the carcinogenic characteristics that some ILs do.[20,21,22,23] Furthermore, HBD components in DESs interact with cations and anions to form complex H-bond networks, which contribute to tunable high thermal stabilities, viscosities and low volatility.[16,17,18,20,23] Such physiochemical properties in DESs should be tunable by varying the HBD and/or ionic salts.[16,17] The ability for these properties to be tuned by a judicious choice of components is appealing as it allows the DESs to be tailored for specific industrial applications such as catalysis, solvent separation, and electrolytes for batteries.[24,25,26,27,28] In particular, a class of DESs that are utilized as rocket propellants are called Deep Eutectic Propellants (DeEPs).[25]

DeEPs are expected to have low vapor pressure, low volatility, and low toxicity compared to energetic IL propellants or hydrazine-based propellants, and to be more economical to produce.[25] Additionally, DeEPs possess properties such as low sensitivities against impact, friction and electrical shock, which are desirable for secure storage and handling and efficiency as a propellant. Thus, it is important to understand the origin of properties related to the impact sensitivity of DeEPs.

A few DeEPs have been prepared and their respective thermodynamic stabilities and impact sensitivities have previously been reported.[25] DeEPs are frequently prepared by mixing a nitrate salt (e.g. ethylammonium nitrate, EAN) and triazole-based heterocyclic ring compounds (e.g. 1-amino-1,2,3-triazole, 1-AT). Evidence from X-ray crystal structures, IR-spectra and thermogravimetric analysis (TGA) suggests that impact sensitivity is related to the nature of H-bonding interactions between EAN and 1-AT. Impact sensitivities can be modified by varying the molar ratio between EAN and 1-AT. In addition, the weakening, breaking and rearranging of intermolecular H-bonds in DeEPs may affect thermodynamic stabilities. For example, both evaporative and decomposition instabilities are observed in EAN and 1-AT based DeEPs; such changes in thermodynamic stabilities could be the result of intermolecular H-bond rearrangements.[25,29] When intermolecular H-bonds are formed or rearranged, two or more H-bonds may strengthen or weaken each other with cooperative and anti-cooperative effects, respectively.[30,31] Water clusters have been widely studied for their H-bonding networks in terms of cooperative and anti-cooperative effects.[30,31,32,33,34] However, those effects are less explored in H-bonded ionic systems despite their importance in structure configurations of molecular clusters of ionic liquids.[35,36] Currently, there is a limited understanding of *why* and *how* intermolecular H-bonds affect the properties of DeEPs.[25,37] To the best of the authors' knowledge, to date, no qualitative or quantitative orbital analysis has been used to investigate the intermolecular H-bonding interactions, especially in the context of cooperative and anti-cooperative effects in DeEPs.

The non-additive character of H-bonds resulting from contributions to the interaction energies can be characterized by energy decomposition methods such as the natural bond orbital (NBO) analysis.[38,39,40] The NBO method can quantitatively analyze intermolecular interaction energies, including those between molecules that are involved in H-bonding. [41,42,43] The NBO analysis suggests that the H-bond strength is related to the charge transfer (CT) energy and proportional to the amount of electron density donated from the filled donor lone-pair orbital into the empty acceptor orbital.[42,44] CT interactions in the NBO analysis are expressed in terms of the overlap between occupied orbitals from the donor and the empty orbitals from the acceptor.[38,45,46] CT in H-bonds plays an important role as an “energy lowering” effect,[47,48] and needs to be evaluated using a highly accurate method.

The effective fragment potential (EFP) method has been shown to provide accurate intermolecular interaction energies, including CT.[4] An EFP is a polarizable force field generated from first principles quantum mechanics with no empirically fitted parameters. [49,50,51,52] The EFP CT interaction energy is defined as the interaction between the valence orbitals of one fragment and the virtual orbitals of another fragment, obtained using second-order Rayleigh Schrodinger perturbation theory.[53,54,55] The EFP method has been shown to be an effective tool for modeling ILs because it captures accurate intermolecular interactions, including those arising from CT interactions.[4,56,57] A benchmark study[4] of EFP IL interaction energies demonstrated reasonable accuracy when compared to symmetry-adapted perturbation theory (SAPT). [46,58]

The recent development of a quasi-atomic (QUAO) bonding analysis [59,60,61,62] method can provide quantitative insight into bond types in terms of orbital occupations, bond orders, and types of orbitals that have bonding interactions. Kinetic bond orders (KBOs) reflect the origin of chemical bonds of interest, as well as the relative strengths of these chemical bonds.[63,64] The method has been used to analyze bonding interactions of various chemical systems, including organic molecules[63], multiple bonding interactions in rhodium monoboride [65], rare gas-containing molecules[66], organozirconium complexes[60,67], and cerium oxides[68]. The method was also employed to study decomposition mechanisms of dioxetane[64]. In addition, the QUAO methodology has been applied to analyze the three-center four-electron interaction of H-bonds in water.[33] Because the EFP method can capture the full range of intermolecular interactions, the energy decomposition in ILs and DeEPs is computed in the present work using the EFP method. The QUAO methodology is then employed to characterize H-bonds in ILs and DeEPs in more detail.

The aim of this study is to elucidate the intermolecular interactions and the H-bond formation in ethyl ammonium nitrate (EAN) and 1-amino-1,2,3 triazole (1-AT)-based DeEP. EAN is chosen as a model DeEP component as it has seen previous wide application as an IL propellant.[69,70,71,72,73,74] 1-AT acts as the HBD for this DeEP. In this study, the most relevant intermolecular interactions of $(EAN)_n$ IL clusters and $(EAN)_x$:$(1\text{-}AT)_n$ (n=1-5) mixtures are studied using the EFP method. The EFP analysis includes noncovalent contributions to intermolecular interactions and H-bond formation in clusters of the type $(EAN)_1$:$(1\text{-}AT)_n$ (n=1-5) and $(EAN)_2$:$(1\text{-}AT)_n$ (n=1-5) DeEP. H-bond formation is further characterized through an analysis of *ab initio* electron density matrices in terms of QUAOs. The relative strengths of H-bonds in the species of interest are analyzed with the aid of KBOs. The methods and theories for the H-bond analysis and intermolecular interactions are summarized in Section 2. The results of the analyses are presented and discussed in Section 3. The conclusions and future directions are presented in Section 4.

2. Computational methods

2.1. Effective Fragment Potential (EFP)

An EFP is a non-empirical polarizable force field generated from first principles quantum mechanics.[49,50,51,52] The EFP method was originally developed to describe aqueous solvent effects on biomolecular systems and chemical reaction mechanisms. More recently, the method has been generalized to evaluate intermolecular interactions in systems such as molecular clusters,[49,51] protein-ligand interactions, [75,76] diffusion in liquids,[77,78] and ILs.[4,79] The EFP method decomposes the fragment-fragment interaction energies into five terms as shown in Eq. (1): Coulomb, charge transfer, exchange repulsion, dispersion and polarization, respectively.[49,50,51,52,54]

$$E_{total}^{EFP} = \sum_{A>B} (E_{AB}^{Coulomb} + E_{AB}^{CT} + E_{AB}^{EXREP} + E_{AB}^{disp}) + E_{AB}^{pol} \qquad (1)$$

The Coulomb, polarization and dispersion terms can be derived from long-range perturbation theory, whereas the exchange-repulsion and charge transfer terms are derived from the overlap of fragment-fragment wave functions. [49,50,51,52,80,54] All of the terms except polarization are pairwise additive. Many-body effects are taken into account through the polarization energy term which is iterated to self-consistency. The EFP method is computationally efficient, free of adjustable parameters, and able to accurately capture the intermolecular interactions between the fragments. [49,50,51,52] The internal geometries of EFPs are fixed and not allowed to relax.

2.2. Quasi-atomic Orbital (QUAO) bonding analysis

The H-bonding in the EAN:$(1\text{-AT})_n$ complexes is analyzed using the quasi-atomic bonding analysis. Since the procedure has been used before,[61,59,64] this section only summarizes the relevant details.

The QUAOs are localized orbitals that may be thought of as free-atom minimal basis set orbitals that have been distorted by the molecular environment.[59,81] The *canonical* QUAOs are obtained by maximizing the overlap of the molecular orbitals onto an accurate atomic minimal basis set (AAMBS) [61,59,64,81]. The AAMBS is determined through a highly accurate self-consistent field calculation on the free atoms.

Based on the AAMBS orbitals, canonical QUAOs are generated for each atom using a singular value decomposition. Then, the canonical QUAOs are orthogonalized preserving the AAMBS orbital characteristics. The orthogonalized canonical QUAOs are then transformed to *oriented* QUAOs by minimizing the number of large bond orders that a given QUAO has with other QUAOs. Hereafter the oriented QUAOs are simply referred to as QUAOs. The QUAO method provides information about bond types (e.g., σ. π), bond orders, and hybridization. The first-order density matrix is expressed in terms of the QUAOs as

$$\rho(1,2) = \sum_{Aa} \sum_{Bb} \left| Aa(1) \rangle p_{Aa,Bb} \langle Bb(2) \right| \tag{2}$$

In Eq. (2) $|Aa\rangle$ is the ath quasi-atomic orbital on atom A. The matrix $p_{Aa,Bb}$ is called the *population/ bond-order-matrix*.[59] The diagonal elements of p_{AaAa} are QUAO occupations. The off-diagonal elements of p_{AaBb} are bond orders (BOs) between orbitals $|Aa\rangle$ and $|Bb\rangle$. The diagonal elements of $p_{Aa,Bb}$ can have values between 0 and 2. The magnitudes of BOs range from 0 to 1.

The QUAO method provides quantitative information about the bond types, bond orders and hybridization characters.[59,64,81] Once the QUAOs are generated, the relative strengths of bonds associated with interacting QUAOs can be estimated using kinetic bond orders (KBOs). Because the origin of covalent bonds is the interference kinetic energy, West and co-workers[64] defined KBOs as the products of the bond orders defined in Eq. (2) and the kinetic energy integrals between interacting QUAOs, scaled by a factor of 0.1 to account for the omission of the potential energy:

$$KBO_{AaBb} = 0.1p_{Aa,Bb}\left\langle Aa\middle|-\frac{1}{2}\nabla^2\middle|Bb\right\rangle \tag{3}$$

KBOs represent the relative strengths of bonds and are always negative for bonding interactions. Bond orders and KBOs are used in this work to analyze H-bonding interactions in DeEP.

2.3. Resolution-of-identity methods

Historically, interaction energies between molecules have been calculated using conventional Moller-Plesset second-order perturbation theory (MP2) and coupled cluster methods, such as CCSD(T). However, conventional MP2 has a steep computational scaling of $\mathcal{O}(\mathrm{N}^5)$where N is the number of basis functions. CCSD(T) has an even steeper $\mathcal{O}(N^7)$ computational scaling.[82,83,84] This makes MP2 and CCSD(T) calculations very challenging for large molecular systems.

The main computational bottleneck of the MP2 method is the evaluation of the $\mathcal{O}(N^4)$ four-center two-electron integrals (ERIs). To address this bottleneck, the resolution-of-the-identity (RI) approximation is introduced. The RI approximation projects the ERIs onto a set of two- and three-center integrals, as shown in Eq. (4), where N_x is the number of auxiliary basis functions[85,86]:

$$(ia|jb) \approx \sum_{PQ}^{N_x}(ia|P)(P|Q)^{-\frac{1}{2}}(Q|jb). \tag{4}$$

In Eq. (4) a,b refer to virtual MOs and i,j denote active occupied MOs. P and Q denote auxiliary basis functions as in reference 85.

Computationally, the final ERIs within the RI approximation can be obtained through highly optimized matrix operations. The RI approximation reduces the cost of the computational bottleneck of MP2 below $\mathcal{O}(N^5)$. In a similar spirit, the RI approximation can also be applied to coupled cluster methods, such as CCSD(T), reducing the $\mathcal{O}(N^7)$ computational cost and (especially) the memory requirements. [83,87,] RI-MP2 and RI-CCSD(T) are significantly faster than conventional MP2 and CCSD(T), respectively, with a negligible loss of accuracy.[83,87,88] In this study, the EFP interaction energies are compared with those obtained via RI-MP2 and RI-CCSD(T).

The *ab initio* interaction energies are calculated following Equation (5).

$$E^{int}(EAN\colon 1AT) = E(EAN\colon 1AT) - E(EAN) - E(1AT) \tag{5}$$

In Eq. (5), $E(EAN\colon 1AT)$ is the *ab initio* (RI-MP2 or RI-CCSD(T)) single point energy of the EAN:1-AT DeEP complex, $E(EAN)$ is the *ab initio* single point energy of EAN, and $E(1AT)$ is the *ab initio* single point energy of 1-amino-1,2,3-triazole.

The *ab initio* interaction energy of the n-body $(EAN)_n$ IL cluster is calculated in a similar manner:

$$E^{int}(EAN)_n = E(EAN)_n - nE(EAN) \tag{6}$$

where $E(EAN)$ is the energy of the EAN monomer, and $E(EAN)_n$ is the *ab initio* single point energy of the n-body EAN cluster.

2.4. Computational details

The structures of the EAN clusters, $(EAN)_1$:$(1\text{-}AT)_n$ (n=1-5) and $(EAN)_2$:$(1\text{-}AT)_n$ (n=1-5) were optimized with the EFP method. Interaction energies were calculated using EFP parameters generated with the 6-311++G(3df,2p) basis set. The EFP interaction energies are compared with RI-MP2/6-311++G(d,p) and RI-CCSD(T)/6-311+G(d,p) interaction energies, using Eqs. (4) and (5). The cc-pVDZ auxiliary basis[85], set is used for the RI-MP2 and RI-CCSD(T) methods. All calculations were carried out using the GAMESS quantum chemistry package.[89,90,91] The QUAO analysis was completed with orbitals obtained using the Hartree-Fock level of theory and visually analyzed using MacMolPlt.[92]

2.5. Geometry optimization

The starting structure of the EAN monomer was directly taken from the EAN crystal structure reported by Henderson *et al.*[93] The EAN cluster structures were then optimized at the EFP level of theory. For the EFP optimization, $[EA]^+$ and $[NO_3]^-$ are considered as two separate fragments that compose the monomer. Then, the nature of the stationary point was confirmed by an EFP hessian calculation. The EFP optimized monomer is the building block of the (EAN)n IL clusters and the $(EAN)_x$: $(1\text{-}AT)_n$ (x=1 or 2, n=1-5) DeEP clusters.

The 1-AT internal geometry was optimized with HF/6-311++G(d,p). The resulting optimized 1-AT monomer geometry is similar to that in the crystal structure reported by Kaplan *et al.*[94]

Monte Carlo (MC) global optimizations

As the cluster size increases, locating the global minimum energy geometry for the cluster becomes difficult due to the existence of many local minima on the potential energy surface.[95,96] In order to locate possible good (low energy) candidates for the computations, EFP Monte Carlo (EFP-MC) global optimizations were carried out. In general, EFP-MC can locate many structures, retaining those that produce energies that are competitive with the energies of structures determined previously. The EFP-MC simulated lowest energy structures for each $(EAN)_n$ IL and DeEP clusters were taken as the most promising structures. Explicit geometry optimizations for the lowest energy structures were performed at the EFP level of theory. The nature of each EFP stationary point was confirmed by an EFP Hessian calculation to verify that there were no imaginary vibrational frequencies.

EFP-MC global optimizations were performed as follows: 10,000 steps were taken to sample geometries. Significant low energy and lowest energy geometries were captured within 250 steps. The simulation temperature follows the Metropolis criterion and evaluated at 20,000K (single simulation temperature). The fragments were allowed to move in a box size of $20\times20\times20$ Å^3. Local geometry optimizations were performed at 0K after every 10 EFP-MC steps.

The details of the EFP-MC global optimizations for each cluster are as follows:

A. *$(EAN)_2$:* The starting geometries of $(EAN)_2$ were constructed by manually positioning two sets of optimized EAN monomers, using the MacMolPlt visualization software.[92] The initial distance between the centers of mass for two optimized EAN monomers was 3.3Å and the monomers were aligned linearly. The lowest energy structure was found and an EFP geometry optimization was performed. EFP Hessian calculations verified that there were no imaginary frequencies. The final inter-monomer distance is 3.75Å.

B. *$(EAN)_n$ (n=4-6):* In order to systematically increase the size of the cluster with uniform inter-monomer distances, the geometry optimized EAN monomers were manually positioned, and the size of the cluster was expanded. For the initial geometries of $(EAN)_4$ and $(EAN)_6$, the monomers were linearly aligned, and the initial distance between the centers of mass for each monomer was set at 3.5 Å.

C. *$(EAN)_n$ (n=8 - 16):* the initial geometries of the clusters were constructed by positioning multiple rows of linearly aligned monomers equal distances apart.

The initial geometries of $(EAN)_{10}$ and $(EAN)_{12}$ were built as two rows of five and six optimized EAN monomers, respectively. The initial geometry of $(EAN)_{16}$ was built as four rows of four optimized EAN monomers. The distance between the centers of mass for two monomers in different rows was taken to be ~ 5.15Å.

By conducting EFP-MC global optimizations from the uniformly ordered crystal structures of $(EAN)_n$ as starting geometries, some rearrangement of the H-bonds in $(EAN)_n$ is expected. Among the geometries examined by the EFP-MC global optimization method, the $(EAN)_n$ structures with the lowest energy were chosen, optimized with EFP, and the obtained stationary points were verified by EFP hessian calculations.

Geometries of $(EAN)_x$: $(1\text{-}AT)_n$ (x=1 or 2, n=1-5) DeEP clusters were also optimized following the analogous steps stated for $(EAN)_n$. For the $(EAN)_1$: $(1\text{-}AT)_1$ cluster, 1-AT molecules were manually positioned such that the centers of mass of the 1-AT and EAN monomer were linearly aligned. For the initial geometries of $(EAN)_2$: $(1\text{-}AT)_1$ cluster, the 1-AT molecules were manually positioned such that the centers of mass of the 1-AT and $(EAN)_2$ formed a triangle shape. The EFP-MC global optimizations were performed. The EFP-MC simulated lowest energy structures were chosen, and then the chosen structures were optimized with EFP.

2.6. Notation for QUAO analysis, populations and bond orders

The QUAO bonding analysis will use the following notation conventions[60]**:** The atomic symbol of the atom on which a QUAO is centered is listed first in capital letters.

Any interaction between two QUAOs with a bond order magnitude greater than 0.1 is considered to be significant. For a significant bonding interaction, the QUAO-centered atom is listed first in capital letters, and the atomic symbol for the partner (complement) atom follows in lower case. An orbital may have more than one complementary atom, as, for example, in three-center bonds. Numerical subscripts for the atomic symbols differentiate between atoms of the same element in the molecule. A QUAO is characterized as σ-bonding, π-bonding, or lone pair, according to a set of criteria introduced by West et al.[84] The symbols σ, π, s, and p indicate that the orbital is a σ-bonding orbital, a π-bonding orbital, an s-type lone pair orbital, or a p-type lone pair orbital, respectively. For the hydrogen bonds (H-bonds), a lower-case h is used to represent an intermolecular H-bond between two atoms. Examples are listed below in Figure 1. The notations are largely adopted from Galvez Vallejo and coworkers[33]:

i. $O_x lp$, $O_x ls$ represents a QUAO that a p-type lone pair and s-type lone pair orbital on oxygen atom *x*, respectively (Figure1a).

ii. $H_x n_y \sigma$ represents a QUAO on hydrogen atom *x* that forms a σ-bond between hydrogen atom *x* and nitrogen atom *y*.

   a. (o) represents a bond to a hydrogen atom that does not participate in a H-bond. For example, $H_x n_y \sigma$(o) describes a sigma bond in which H_x does not form a hydrogen bond. (Figure 1b)
   b. (i) represents a bond to a hydrogen atom that does participate in a H-bond. For example, $H_x n_y \sigma$(i) describes a sigma bond within $[EA]^+$ in which H_x participates in a hydrogen bond. (Figure 1c)

iii. $H_x o_y h$ represents a QUAO on a hydrogen atom *x* that participates in a hydrogen bond with oxygen atom *y* (Figure 1d). Similarly, $H_x n_y h$ represents a QUAO on a hydrogen atom *x* that forms a hydrogen bond between hydrogen atom *x* and nitrogen atom *y*. (Figure 1e).
   a. The type of lone pair is indicated as follows: $H_x o_{y,pl} h$ represents an intermolecular H-bond between the hydrogen atom *x* and the p-type lone pair of oxygen atom *y*, whereas $H_x o_{y,sl} h$ represents an intermolecular H-bond between the hydrogen atom *x* and the s-type lone pair of oxygen atom *y*.

iv. $H_x - o_y - h_z AT$ represents a network of H-bonds: hydrogen atoms *x* and *z* form two separate intermolecular H-bonds with $[NO_3]^-$ and 1-AT. Oxygen atom y is "bridging" two hydrogen atoms and forming a network. The first H-bond is formed between hydrogen atom *x* and oxygen atom *y* from $[NO_3]^-$. The second H-bond is found between hydrogen atom *z* from the 1-AT molecule and oxygen atom *y*.

v. An example of a double donor is an ethylammonium cation ($[EA]^+$), whose two hydrogen atoms in the amino group participate in H-bonding. (Figure 1f)
   a. A double donor bond can be labelled $N_x h_{y(z)} h$, which means that nitrogen atom *x* is bonded to hydrogen atoms *y* and *z*, which are involved in H-bonds.

vi. An example of a double acceptor is a $[NO_3]^-$, whose oxygen atom accepts two H-bonds. (Figure 1g)

   a. A double acceptor bond can be labeled as $H_{x(y)}o_z h$, which indicates that the oxygen atom z is accepting H-bonds from hydrogen atoms x and y.

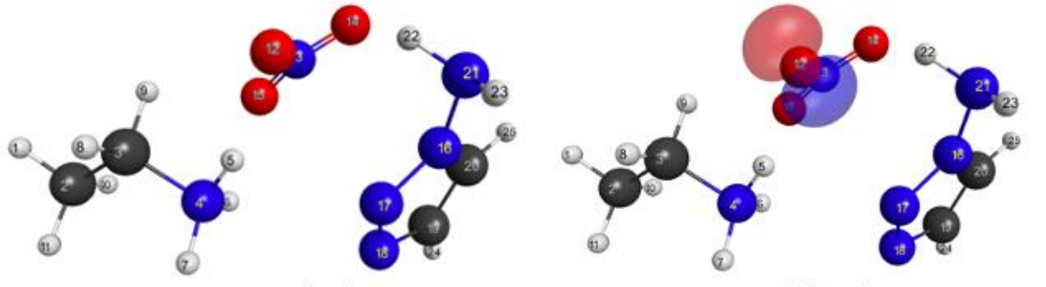

EAN monomer : (1-AT)$_1$ (a) O$_{12}$*pl*

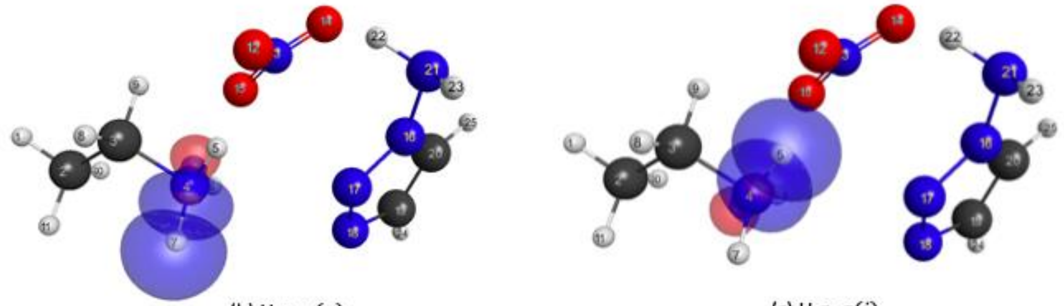

(b) H$_7$n$_4\sigma(o)$ (c) H$_7$n$_4\sigma(i)$

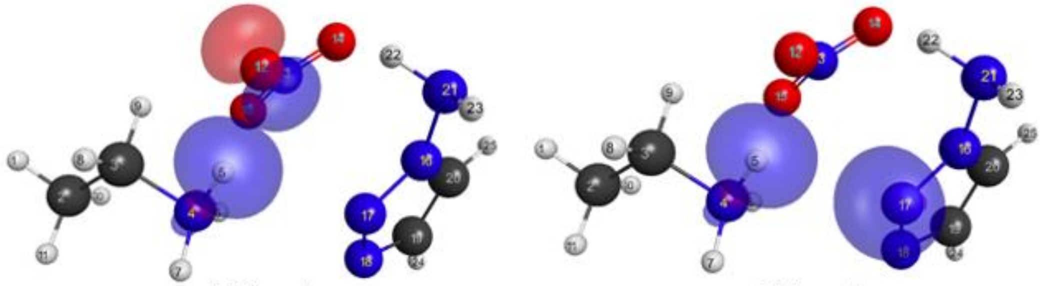

(d) H$_5$o$_{12pl}$h (e) H$_5$n$_{17,pl}$h

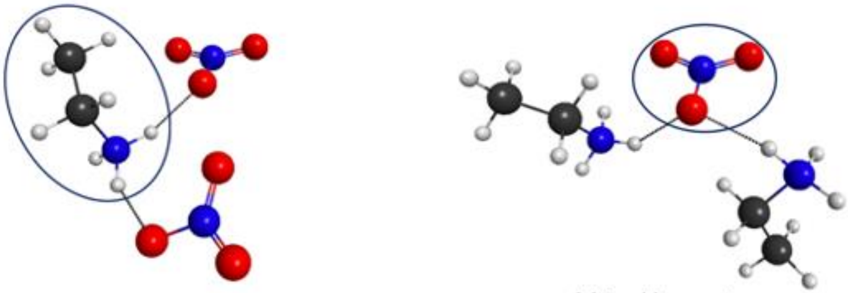

(f) Double donor (g) Double acceptor

Figure 1. Notation examples for QUAOs in EAN:(1-AT)$_1$. The atom labels follow the numbering designated in the geometry of EAN:(1-AT)$_1$ in the box at the upper left. (a) QUAO of oxygen p-type lone

pair (b) sigma bond formation depicted by QUAOs of hydrogen (H7) and nitrogen (N4). H7 does not participate in a H-bond (c) sigma bond formation depicted by QUAOs of hydrogen (H5) and nitrogen (N4). H5 does not participate in a H-bond (d) H-bonding interaction described by QUAO of hydrogen (H5) and the QUAO of p-type lone pair on the oxygen atom (O12). (e) H-bonding interaction between QUAO of hydrogen (H5) and the QUAO of p-type lone pair on the nitrogen atom (N17). (f) an example of double donor configuration (g) an example of double acceptor configuration

3. Results and Discussion

The EFP optimized geometries for the EAN clusters and for the $(EAN)_x$: $(1\text{-}AT)_n$ (x=1 or 2, n=1-5) clusters are shown in shown in **Figures 2 through 13**, respectively.

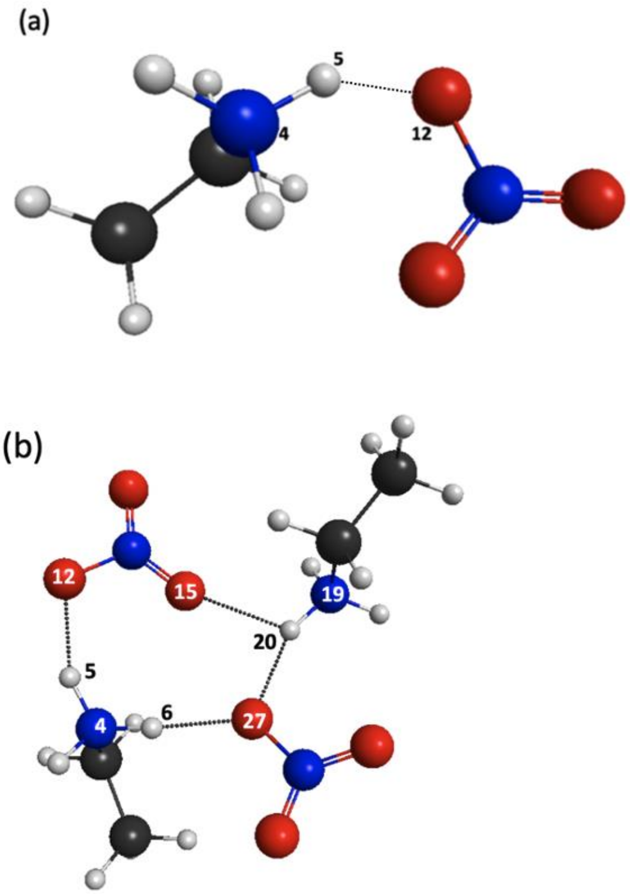

(EAN)$_1$		
Bonds	R_{H-bond} (Å)	Θ_{H-bond} (Degree)
H5···O12 (sd,sa)	1.75	155.99
Average	1.75 Å	155.99 °

(EAN)$_2$		
Bonds	R_{H-bond} (Å)	Θ_{H-bond} (Degree)
H5···O12(sd,sa)	1.75	155.99
Average	1.75 Å	155.99 °

Figure 2. EFP-optimized geometries of (a) $(EAN)_1$ (b) $(EAN)_2$. Atoms that have H-bonding interactions are indicated by atom numbers and listed under "Bonds". Hydrogen bonds are indicated with dotted lines. R_{H-bond} represents the distance between a hydrogen atom from $[EA]^+$ and an oxygen atom from $[NO_3]^-$ that form a H-bond. Units are in Å. Θ_{H-bond} is the angle measured in ethylammonium N-H···O (nitrate). *dd* and *sd* indicate a hydrogen atom in double donor or single donor arrangement. *da* and *sa* indicate an oxygen atom in a double acceptor or single acceptor arrangement. For example, $H_x\cdots O_y$ (*dd*,*da*) represents a H-bond between H_x and O_y where H_x is a hydrogen atom from a double donor, and O_y is an oxygen atom from a double acceptor.

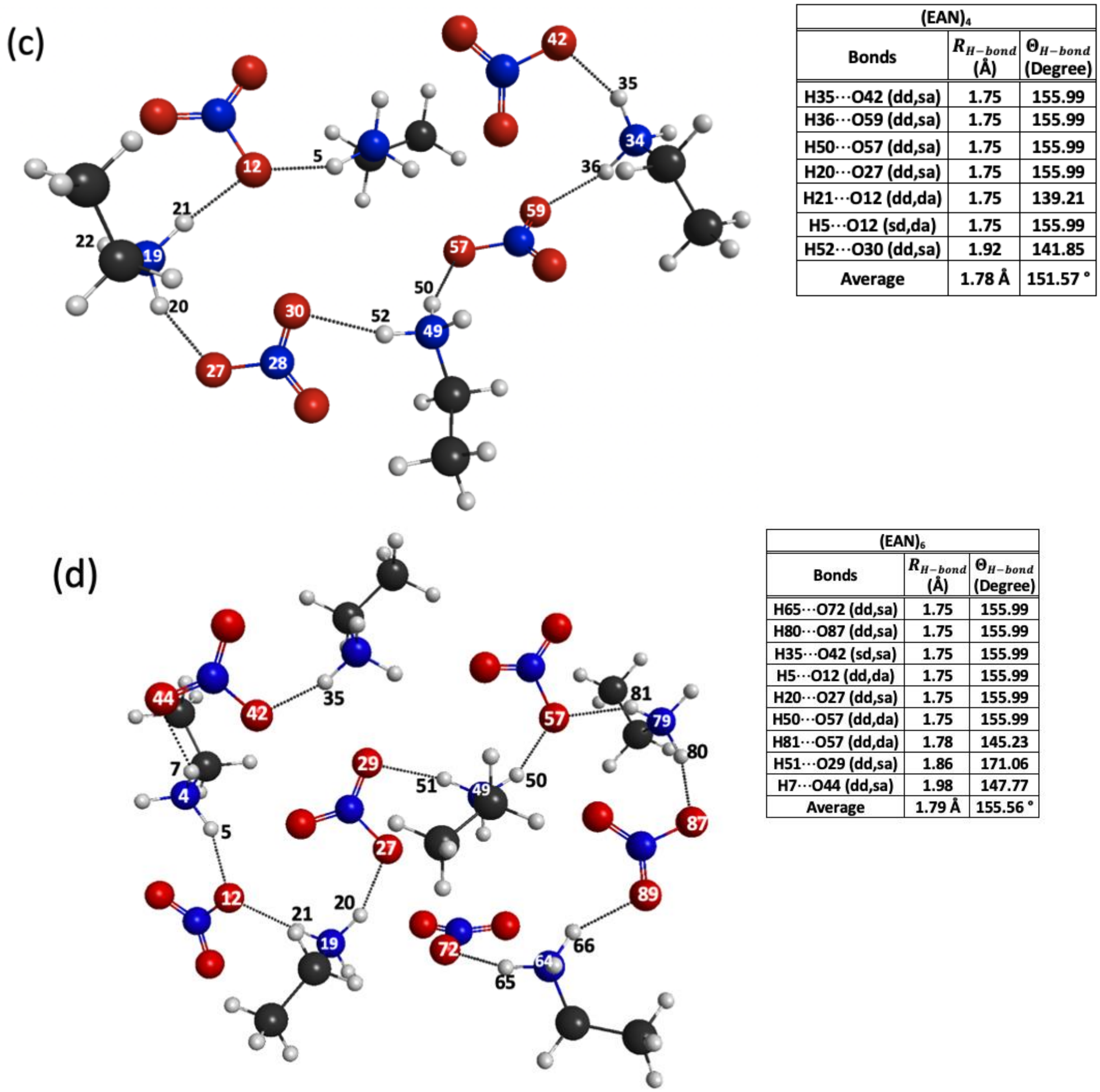

(EAN)$_4$		
Bonds	R_{H-bond} (Å)	Θ_{H-bond} (Degree)
H35···O42 (dd,sa)	1.75	155.99
H36···O59 (dd,sa)	1.75	155.99
H50···O57 (dd,sa)	1.75	155.99
H20···O27 (dd,sa)	1.75	155.99
H21···O12 (dd,da)	1.75	139.21
H5···O12 (sd,da)	1.75	155.99
H52···O30 (dd,sa)	1.92	141.85
Average	1.78 Å	151.57 °

(EAN)$_6$		
Bonds	R_{H-bond} (Å)	Θ_{H-bond} (Degree)
H65···O72 (dd,sa)	1.75	155.99
H80···O87 (dd,sa)	1.75	155.99
H35···O42 (sd,sa)	1.75	155.99
H5···O12 (dd,da)	1.75	155.99
H20···O27 (dd,sa)	1.75	155.99
H50···O57 (dd,da)	1.75	155.99
H81···O57 (dd,da)	1.78	145.23
H51···O29 (dd,sa)	1.86	171.06
H7···O44 (dd,sa)	1.98	147.77
Average	1.79 Å	155.56 °

Figure 3. EFP-optimized geometries of (c) $(EAN)_4$ (d) $(EAN)_6$. Atoms that have H-bonding interactions are indicated by atom numbers and listed under "Bonds". Hydrogen bonds are indicated with dotted lines. R_{H-bond} represents the distance between a hydrogen atom from $[EA]^+$ and an oxygen atom from $[NO_3]^-$ that form a H-bond. Units are in Å. Θ_{H-bond} is the angle measured in ethylammonium N-H···O (nitrate). *dd* and *sd* indicate a hydrogen atom in double donor or single donor arrangement. *da* and *sa* indicate an oxygen atom in a double acceptor or single acceptor arrangement. For example, $H_x \cdots O_y$ (*dd*,*da*) represents a H-bond between H_x and O_y where H_x is a hydrogen atom from a double donor, and O_y is an oxygen atom from a double acceptor.

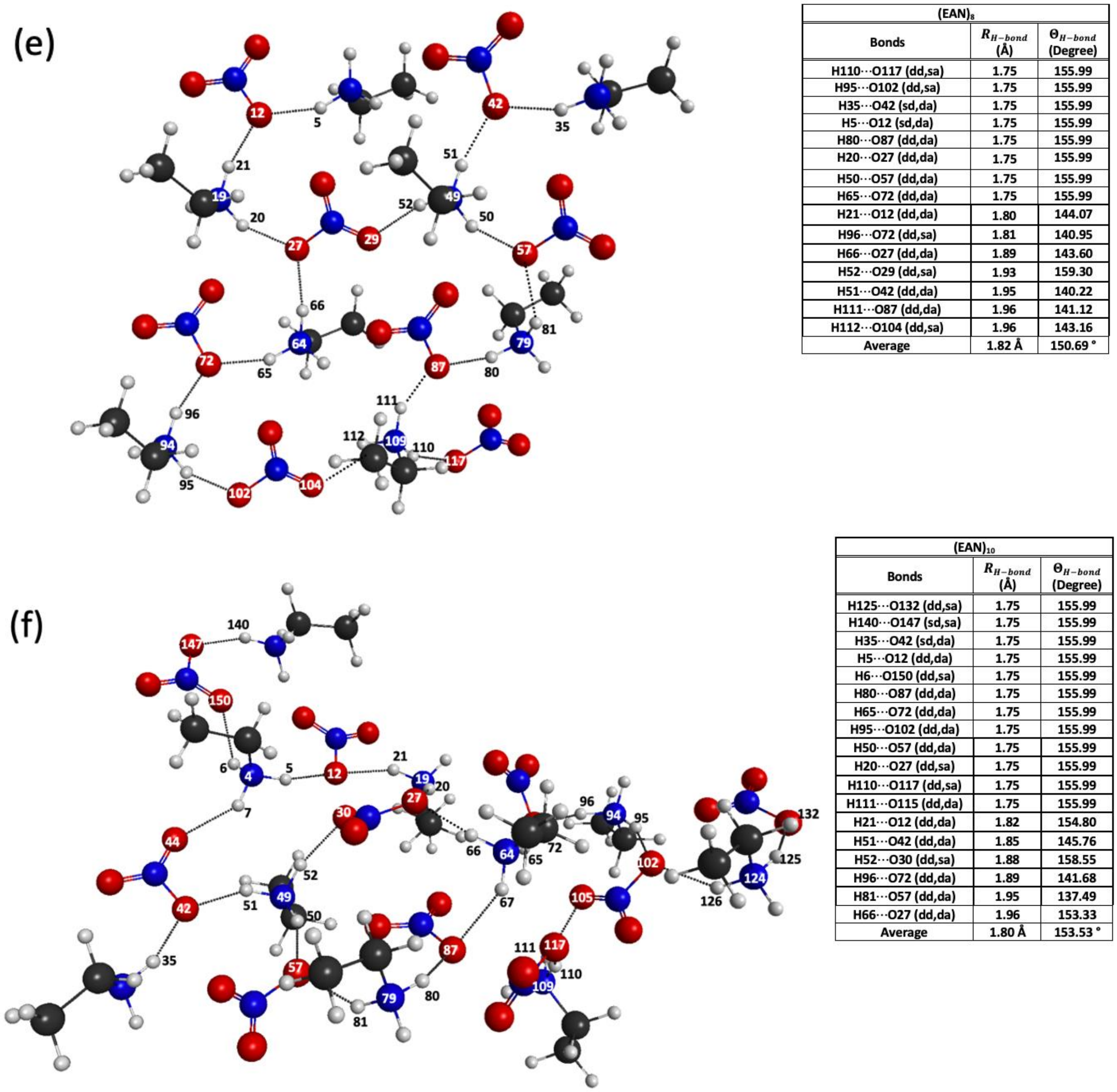

(EAN)$_8$		
Bonds	R_{H-bond} (Å)	Θ_{H-bond} (Degree)
H110···O117 (dd,sa)	1.75	155.99
H95···O102 (dd,sa)	1.75	155.99
H35···O42 (sd,da)	1.75	155.99
H5···O12 (sd,da)	1.75	155.99
H80···O87 (dd,da)	1.75	155.99
H20···O27 (dd,da)	1.75	155.99
H50···O57 (dd,da)	1.75	155.99
H65···O72 (dd,da)	1.75	155.99
H21···O12 (dd,da)	1.80	144.07
H96···O72 (dd,sa)	1.81	140.95
H66···O27 (dd,da)	1.89	143.60
H52···O29 (dd,sa)	1.93	159.30
H51···O42 (dd,da)	1.95	140.22
H111···O87 (dd,da)	1.96	141.12
H112···O104 (dd,sa)	1.96	143.16
Average	1.82 Å	150.69 °

(EAN)$_{10}$		
Bonds	R_{H-bond} (Å)	Θ_{H-bond} (Degree)
H125···O132 (dd,sa)	1.75	155.99
H140···O147 (sd,sa)	1.75	155.99
H35···O42 (sd,da)	1.75	155.99
H5···O12 (dd,da)	1.75	155.99
H6···O150 (dd,sa)	1.75	155.99
H80···O87 (dd,da)	1.75	155.99
H65···O72 (dd,da)	1.75	155.99
H95···O102 (dd,da)	1.75	155.99
H50···O57 (dd,da)	1.75	155.99
H20···O27 (dd,sa)	1.75	155.99
H110···O117 (dd,sa)	1.75	155.99
H111···O115 (dd,da)	1.75	155.99
H21···O12 (dd,da)	1.82	154.80
H51···O42 (dd,da)	1.85	145.76
H52···O30 (dd,sa)	1.88	158.55
H96···O72 (dd,da)	1.89	141.68
H81···O57 (dd,da)	1.95	137.49
H66···O27 (dd,da)	1.96	153.33
Average	1.80 Å	153.53 °

Figure 4. EFP-optimized geometries of (e) (EAN)$_8$ and (f) (EAN)$_{10}$. Atoms that have H-bonding interactions are indicated by atom numbers and listed under "Bonds". Hydrogen bonds are indicated with dotted lines. R_{H-bond} represents the distance between a hydrogen atom from $[EA]^+$ and an oxygen atom from $[NO_3]^-$ that form a H-bond. Units are in Å. Θ_{H-bond} is the angle measured in ethylammonium N-H···O (nitrate). *dd* and *sd* indicate a hydrogen atom in double donor or single donor arrangement. *da* and *sa* indicate an oxygen atom in a double acceptor or single acceptor arrangement. For example, H_x···O_y (*dd*,*da*) represents a H-bond between H_x and O_y where H_x is a hydrogen atom from a double donor, and O_y is an oxygen atom from a double acceptor.

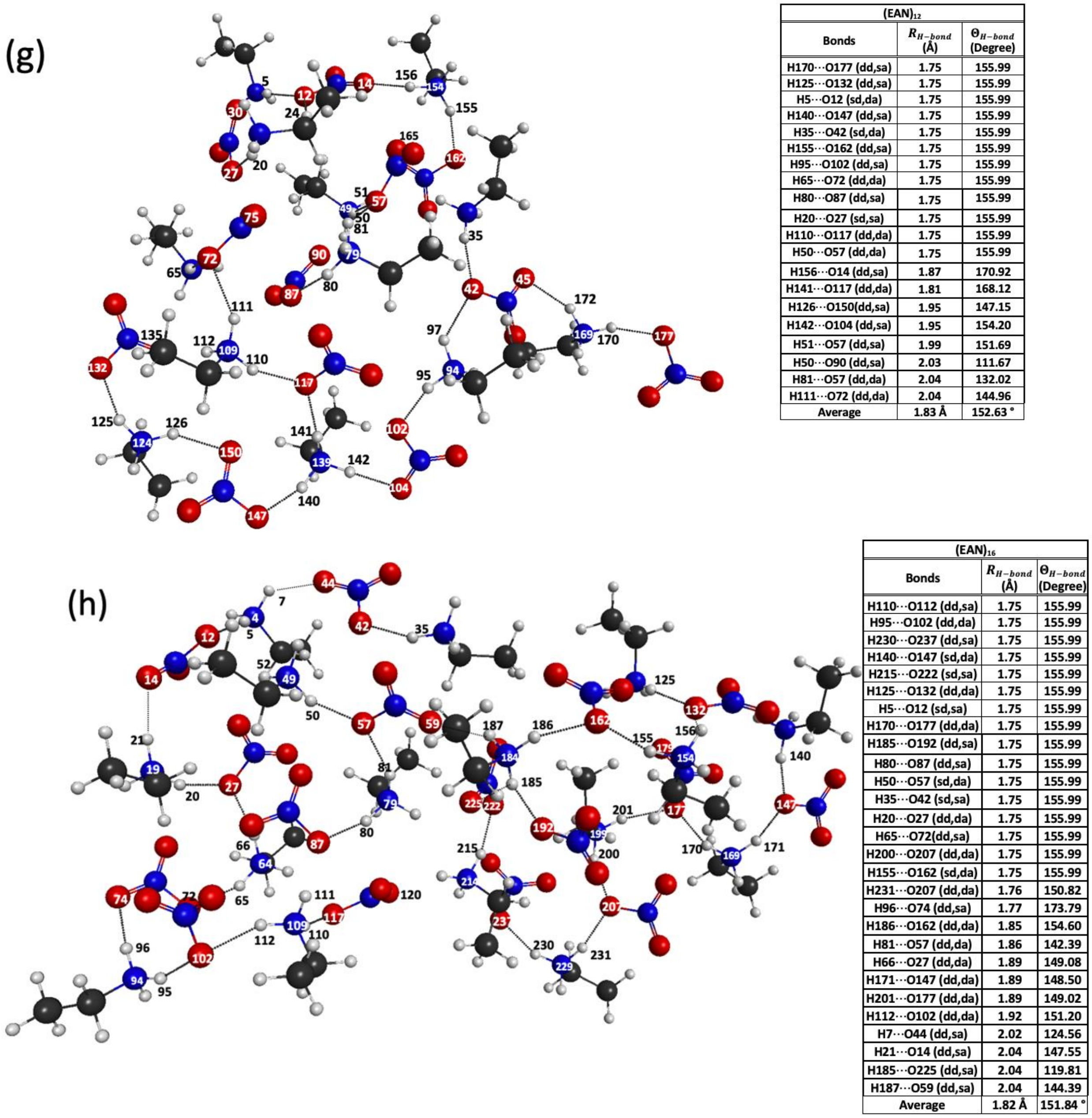

(EAN)$_{12}$		
Bonds	R_{H-bond} (Å)	Θ_{H-bond} (Degree)
H170···O177 (dd,sa)	1.75	155.99
H125···O132 (dd,sa)	1.75	155.99
H5···O12 (sd,da)	1.75	155.99
H140···O147 (dd,sa)	1.75	155.99
H35···O42 (sd,da)	1.75	155.99
H155···O162 (dd,sa)	1.75	155.99
H95···O102 (dd,sa)	1.75	155.99
H65···O72 (dd,da)	1.75	155.99
H80···O87 (dd,sa)	1.75	155.99
H20···O27 (sd,sa)	1.75	155.99
H110···O117 (dd,da)	1.75	155.99
H50···O57 (dd,da)	1.75	155.99
H156···O14 (dd,sa)	1.87	170.92
H141···O117 (dd,da)	1.81	168.12
H126···O150(dd,sa)	1.95	147.15
H142···O104 (dd,sa)	1.95	154.20
H51···O57 (dd,sa)	1.99	151.69
H50···O90 (dd,sa)	2.03	111.67
H81···O57 (dd,da)	2.04	132.02
H111···O72 (dd,da)	2.04	144.96
Average	1.83 Å	152.63 °

(EAN)$_{16}$		
Bonds	R_{H-bond} (Å)	Θ_{H-bond} (Degree)
H110···O112 (dd,sa)	1.75	155.99
H95···O102 (dd,da)	1.75	155.99
H230···O237 (dd,sa)	1.75	155.99
H140···O147 (sd,da)	1.75	155.99
H215···O222 (sd,sa)	1.75	155.99
H125···O132 (dd,da)	1.75	155.99
H5···O12 (sd,sa)	1.75	155.99
H170···O177 (dd,da)	1.75	155.99
H185···O192 (dd,sa)	1.75	155.99
H80···O87 (dd,sa)	1.75	155.99
H50···O57 (sd,da)	1.75	155.99
H35···O42 (sd,sa)	1.75	155.99
H20···O27 (dd,da)	1.75	155.99
H65···O72(dd,sa)	1.75	155.99
H200···O207 (dd,da)	1.75	155.99
H155···O162 (sd,da)	1.75	155.99
H231···O207 (dd,da)	1.76	150.82
H96···O74 (dd,sa)	1.77	173.79
H186···O162 (dd,da)	1.85	154.60
H81···O57 (dd,da)	1.86	142.39
H66···O27 (dd,da)	1.89	149.08
H171···O147 (dd,da)	1.89	148.50
H201···O177 (dd,da)	1.89	149.02
H112···O102 (dd,da)	1.92	151.20
H7···O44 (dd,sa)	2.02	124.56
H21···O14 (dd,sa)	2.04	147.55
H185···O225 (dd,sa)	2.04	119.81
H187···O59 (dd,sa)	2.04	144.39
Average	1.82 Å	151.84 °

Figure 5. EFP-optimized geometries of (g) $(EAN)_{12}$ and (h) $(EAN)_{16}$. Atoms that have H-bonding interactions are indicated by atom numbers and listed under "Bonds". Hydrogen bonds are indicated with dotted lines. R_{H-bond} represents the distance between a hydrogen atom from $[EA]^+$ and an oxygen atom from $[NO_3]^-$ that form a H-bond. Units are in Å. Θ_{H-bond} is the angle measured in ethylammonium N-H···O (nitrate). *dd* and *sd* indicate a hydrogen atom in double donor or single donor arrangement. *da* and *sa* indicate an oxygen atom in a double acceptor or single acceptor arrangement. For example, $H_x \cdots O_y$ (*dd*,*da*) represents a H-bond between H_x and O_y where H_x is a hydrogen atom from a double donor, and O_y is an oxygen atom from a double acceptor.

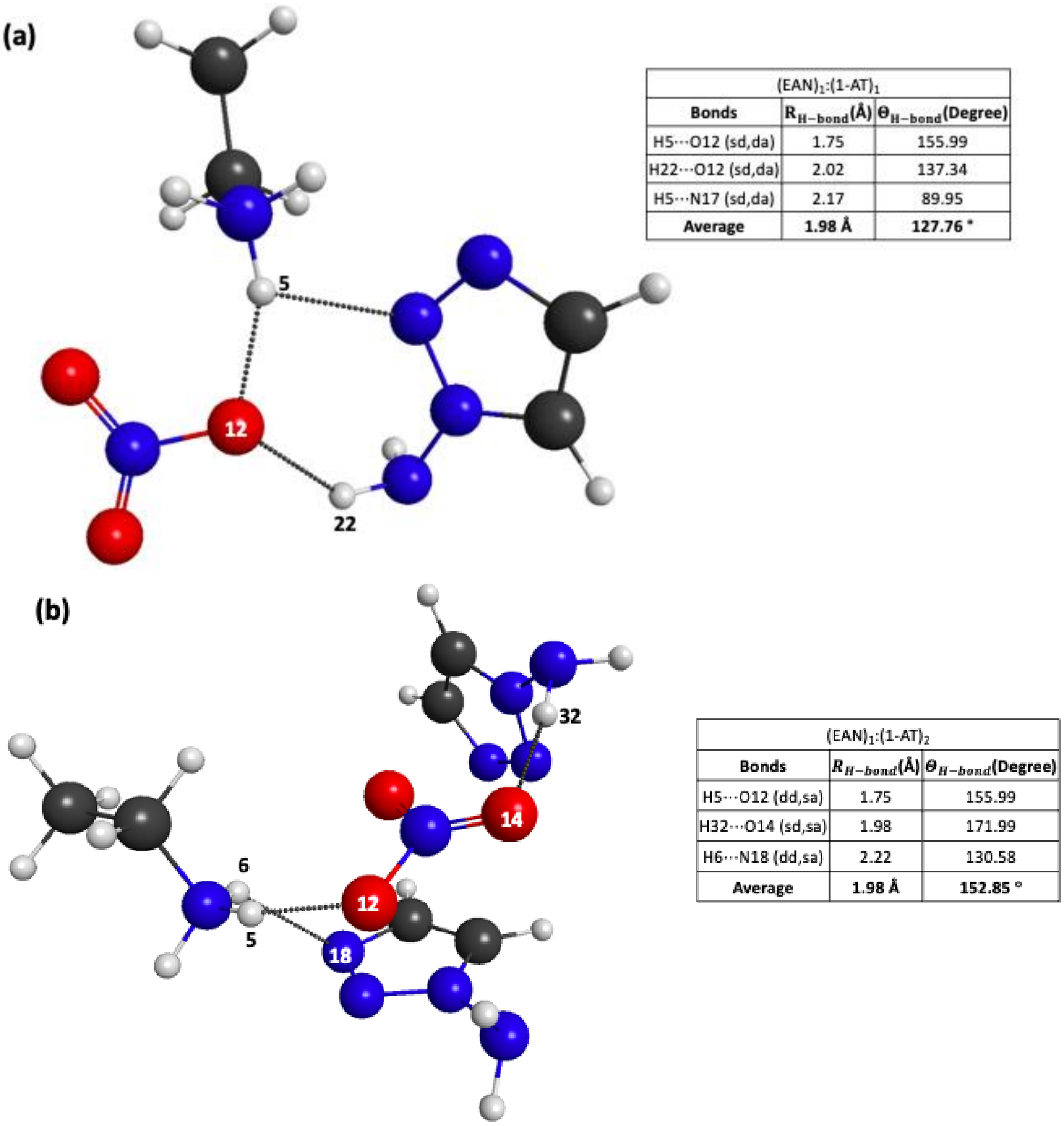

$(EAN)_1:(1\text{-}AT)_1$		
Bonds	**R_{H-bond}(Å)**	**Θ_{H-bond}(Degree)**
H5···O12 (sd,da)	1.75	155.99
H22···O12 (sd,da)	2.02	137.34
H5···N17 (sd,da)	2.17	89.95
Average	**1.98 Å**	**127.76 °**

$(EAN)_1:(1\text{-}AT)_2$		
Bonds	**R_{H-bond}(Å)**	**Θ_{H-bond}(Degree)**
H5···O12 (dd,sa)	1.75	155.99
H32···O14 (sd,sa)	1.98	171.99
H6···N18 (dd,sa)	2.22	130.58
Average	**1.98 Å**	**152.85 °**

Figure 6. EFP Optimized geometries for $(EAN)_1:(1\text{-}AT)_n$ (n=1,2). Atoms that have H-bonding interactions are indicated by atom numbers and listed under "Bonds". Hydrogen bonds are indicated with dotted lines. R_{H-bond} represents the H-bond distance. Units are in Å. Θ_{H-bond} is the H-bond angle measured in 1) ethylammonium N-H···O (nitrate), 2) 1-AT N-H···O (nitrate), 3) ethylammonium N-H···N (1-AT), or 4) 1-AT N-H···N (1-AT). *dd* and *sd* indicate a hydrogen atom in a double donor or single donor arrangement. *da* and *sa* indicate an oxygen atom in a double acceptor or single acceptor arrangement. For example, $H_x\cdots O_y$ (*dd,da*) represents a H-bond between H_x and O_y where H_x is a hydrogen atom from a double donor, and O_y is an oxygen atom from a double acceptor.

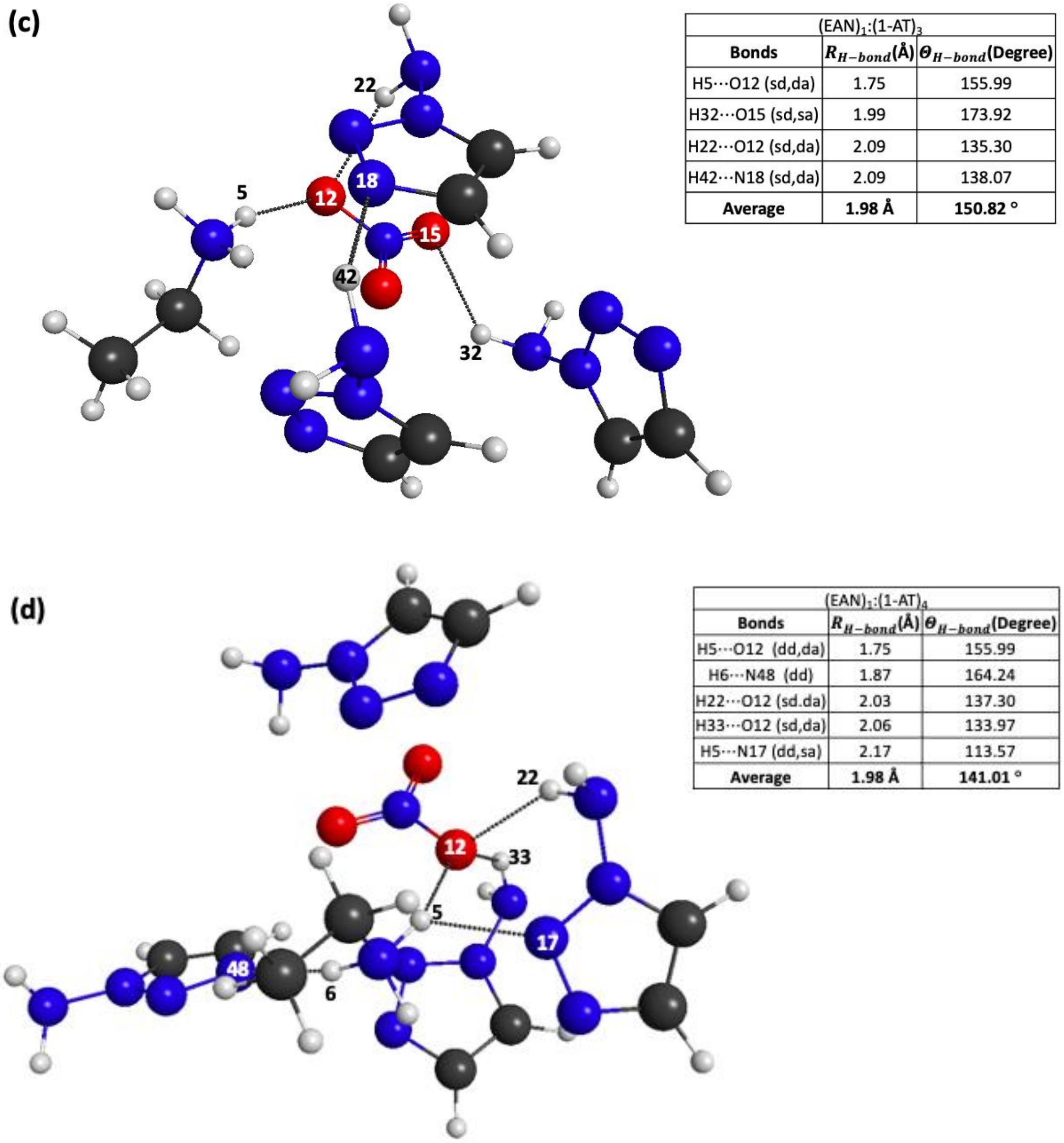

(EAN)$_1$:(1-AT)$_3$		
Bonds	R_{H-bond}(Å)	Θ_{H-bond}(Degree)
H5···O12 (sd,da)	1.75	155.99
H32···O15 (sd,sa)	1.99	173.92
H22···O12 (sd,da)	2.09	135.30
H42···N18 (sd,da)	2.09	138.07
Average	**1.98 Å**	**150.82 °**

(EAN)$_1$:(1-AT)$_4$		
Bonds	R_{H-bond}(Å)	Θ_{H-bond}(Degree)
H5···O12 (dd,da)	1.75	155.99
H6···N48 (dd)	1.87	164.24
H22···O12 (sd.da)	2.03	137.30
H33···O12 (sd,da)	2.06	133.97
H5···N17 (dd,sa)	2.17	113.57
Average	**1.98 Å**	**141.01 °**

Figure 7. EFP Optimized geometries for (EAN)$_1$:(1-AT)$_n$ (n=3,4). Atoms that have H-bonding interactions are indicated by atom numbers and listed under "Bonds". Hydrogen bonds are indicated with dotted lines. R_{H-bond} represents the H-bond distance. Units are in Å. Θ_{H-bond} is the H-bond angle measured in 1) ethylammonium N-H···O (nitrate), 2) 1-AT N-H···O (nitrate), 3) ethylammonium N-H···N (1-AT), or 4) 1-AT N-H···N (1-AT). *dd* and *sd* indicate a hydrogen atom in a double donor or single donor arrangement. *da* and *sa* indicate an oxygen atom in a double acceptor or single acceptor arrangement. For example, H$_x$···O$_y$ (*dd,da*) represents a H-bond between H$_x$ and O$_y$ where H$_x$ is a hydrogen atom from a double donor, and O$_y$ is an oxygen atom from a double acceptor.

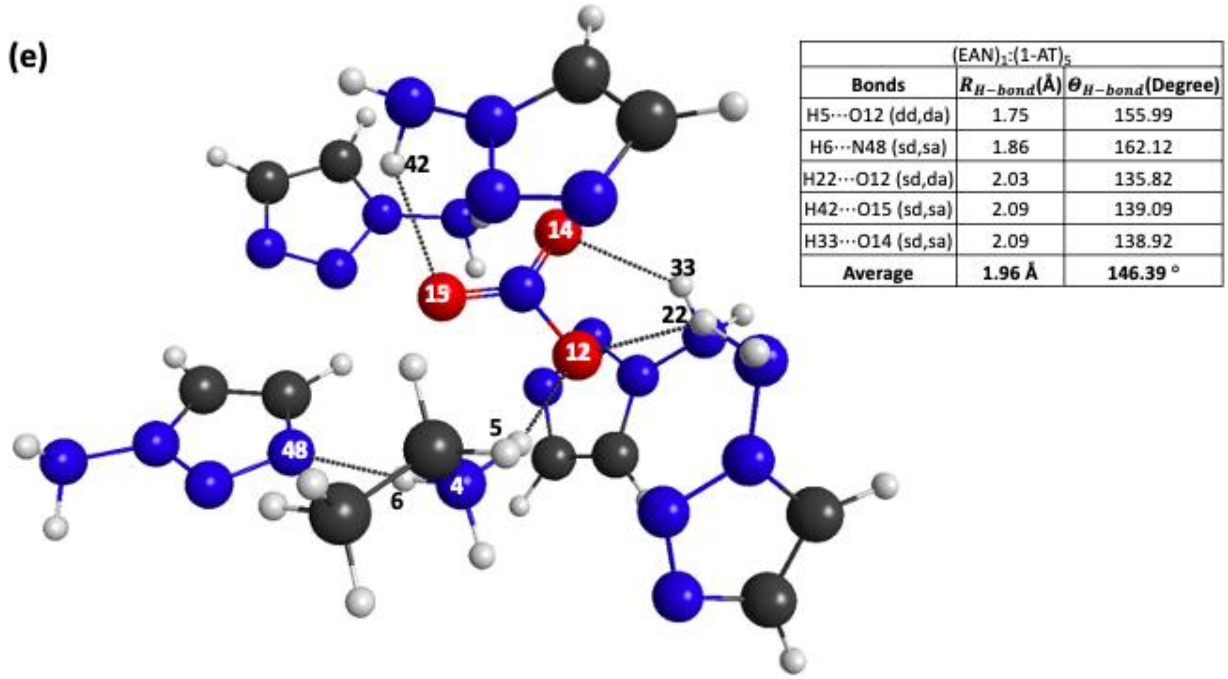

(EAN)$_1$:(1-AT)$_5$		
Bonds	R_{H-bond}(Å)	Θ_{H-bond}(Degree)
H5···O12 (dd,da)	1.75	155.99
H6···N48 (sd,sa)	1.86	162.12
H22···O12 (sd,da)	2.03	135.82
H42···O15 (sd,sa)	2.09	139.09
H33···O14 (sd,sa)	2.09	138.92
Average	**1.96 Å**	**146.39 °**

Figure 8. EFP Optimized geometries for (EAN)$_1$:(1-AT)$_n$ (n=5). Atoms that have H-bonding interactions are indicated by atom numbers and listed under "Bonds". Hydrogen bonds are indicated with dotted lines. R_{H-bond} represents the H-bond distance. Units are in Å. Θ_{H-bond} is the H-bond angle measured in 1) ethylammonium N-H···O (nitrate), 2) 1-AT N-H···O (nitrate), 3) ethylammonium N-H···N (1-AT), or 4) 1-AT N-H···N (1-AT). *dd* and *sd* indicate a hydrogen atom in a double donor or single donor arrangement. *da* and *sa* indicate an oxygen atom in a double acceptor or single acceptor arrangement. For example, $H_x···O_y$ (*dd,da*) represents a H-bond between H_x and O_y where H_x is a hydrogen atom from a double donor, and O_y is an oxygen atom from a double acceptor.

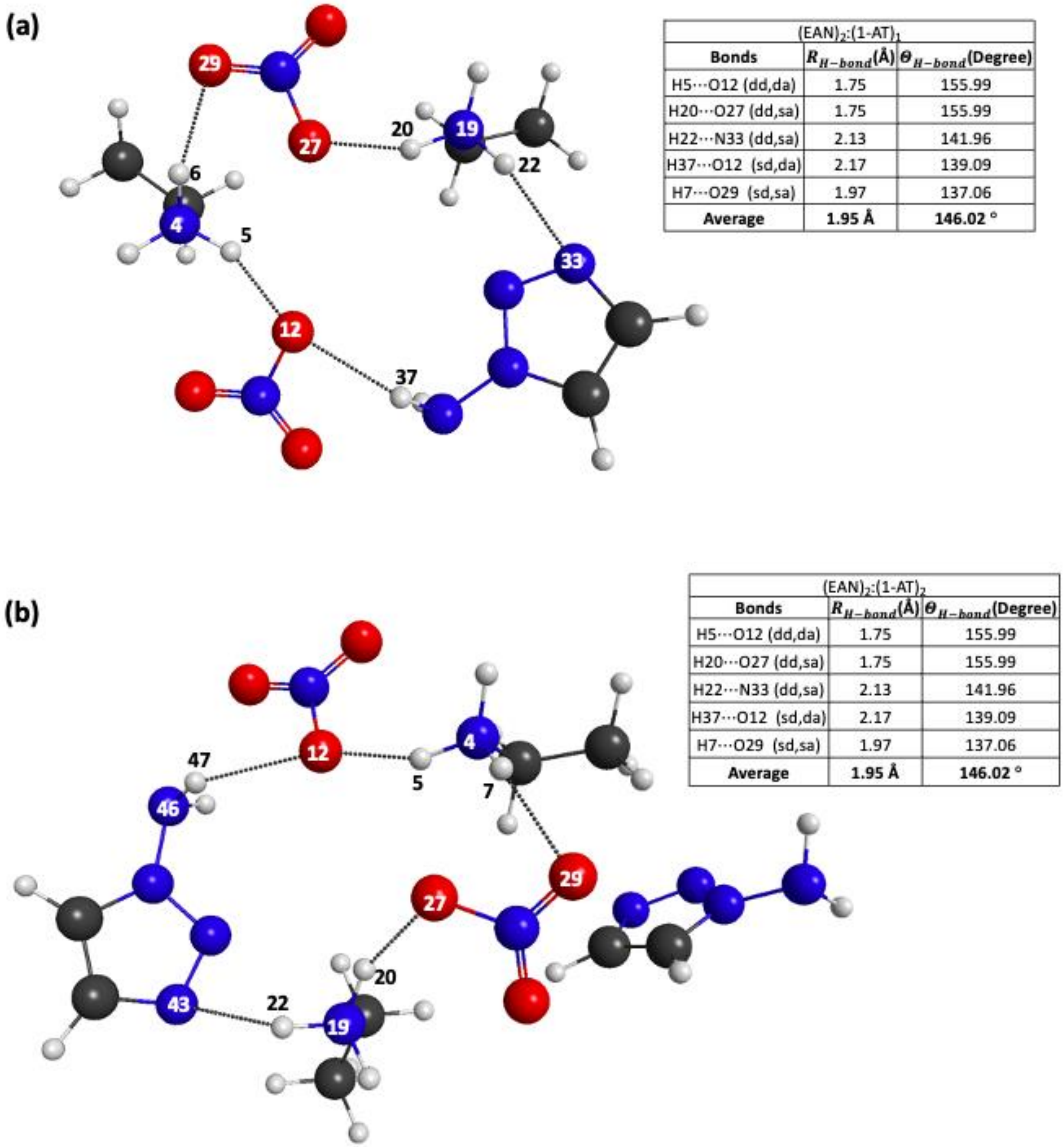

(EAN)$_2$:(1-AT)$_1$

Bonds	R_{H-bond}(Å)	Θ_{H-bond}(Degree)
H5···O12 (dd,da)	1.75	155.99
H20···O27 (dd,sa)	1.75	155.99
H22···N33 (dd,sa)	2.13	141.96
H37···O12 (sd,da)	2.17	139.09
H7···O29 (sd,sa)	1.97	137.06
Average	**1.95 Å**	**146.02 °**

(EAN)$_2$:(1-AT)$_2$

Bonds	R_{H-bond}(Å)	Θ_{H-bond}(Degree)
H5···O12 (dd,da)	1.75	155.99
H20···O27 (dd,sa)	1.75	155.99
H22···N33 (dd,sa)	2.13	141.96
H37···O12 (sd,da)	2.17	139.09
H7···O29 (sd,sa)	1.97	137.06
Average	**1.95 Å**	**146.02 °**

Figure 9. EFP Optimized geometries for (EAN)$_2$:(1-AT)$_n$ (n=1,2). Atoms that have H-bonding interactions are indicated by atom numbers and listed under "Bonds". Hydrogen bonds are indicated with dotted lines. R_{H-bond} represents the H-bond distance. Units are in Å. Θ_{H-bond} is the H-bond angle measured in ethylammonium N-H···O (nitrate), 1-AT N-H···O (nitrate), or ethylammonium N-H···N (1-AT). *dd* and *sd* indicate a hydrogen atom in a double donor or a single donor arrangement. *da* and *sa* indicate an oxygen atom in a double acceptor or a single acceptor arrangement. For example, H_x···O_y (*dd,da*) represents a H-bond between H_x and O_y where H_x is a hydrogen atom from a double donor, and O_y is an oxygen atom from a double acceptor

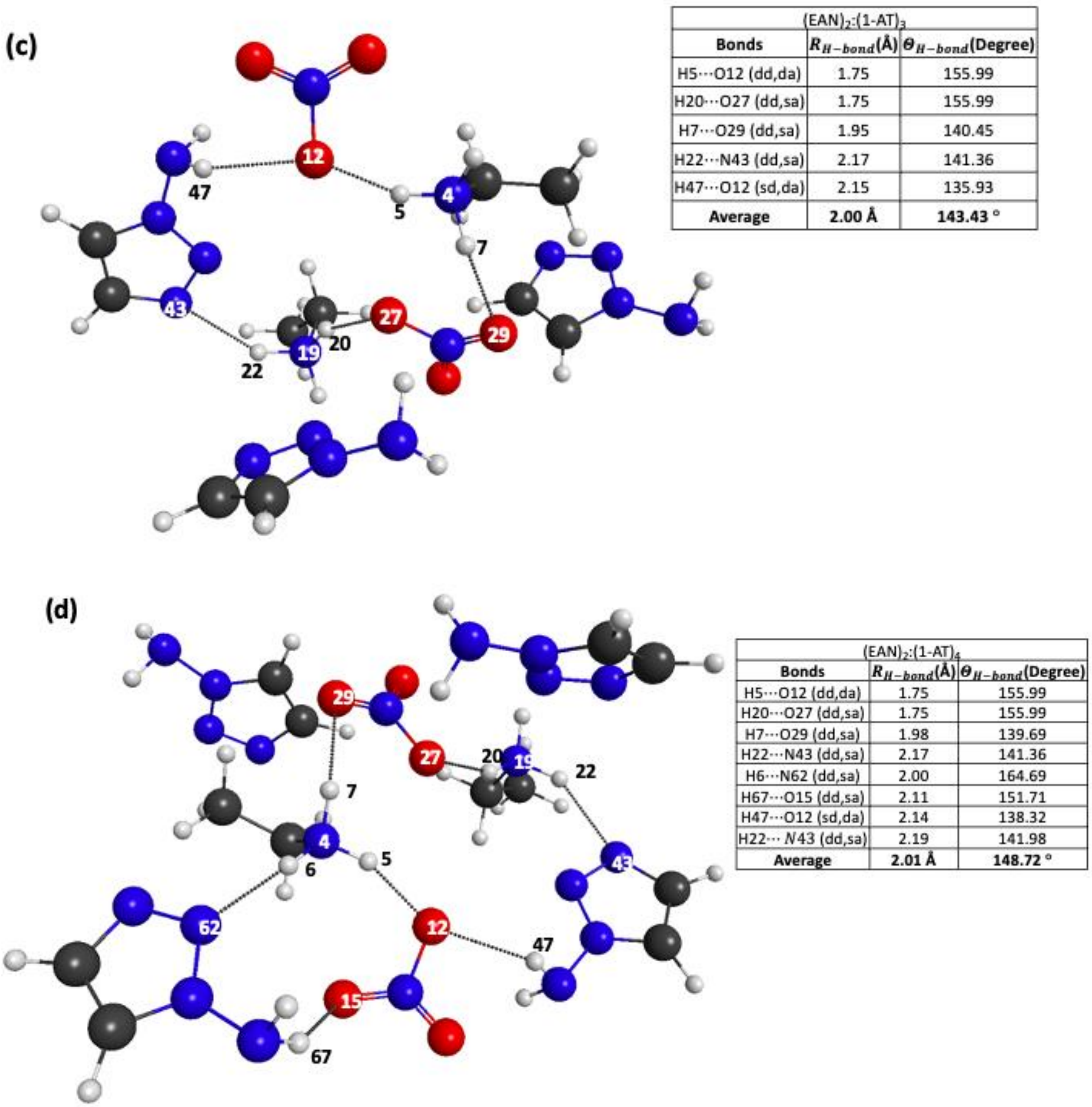

$(EAN)_2$:(1-AT)$_3$		
Bonds	R_{H-bond}**(Å)**	Θ_{H-bond}**(Degree)**
H5···O12 (dd,da)	1.75	155.99
H20···O27 (dd,sa)	1.75	155.99
H7···O29 (dd,sa)	1.95	140.45
H22···N43 (dd,sa)	2.17	141.36
H47···O12 (sd,da)	2.15	135.93
Average	**2.00 Å**	**143.43 °**

$(EAN)_2$:(1-AT)$_4$		
Bonds	R_{H-bond}**(Å)**	Θ_{H-bond}**(Degree)**
H5···O12 (dd,da)	1.75	155.99
H20···O27 (dd,sa)	1.75	155.99
H7···O29 (dd,sa)	1.98	139.69
H22···N43 (dd,sa)	2.17	141.36
H6···N62 (dd,sa)	2.00	164.69
H67···O15 (dd,sa)	2.11	151.71
H47···O12 (sd,da)	2.14	138.32
H22··· N43 (dd,sa)	2.19	141.98
Average	**2.01 Å**	**148.72 °**

Figure 10. EFP Optimized geometries for $(EAN)_2:(1\text{-}AT)_n$ (n=3,4). Atoms that have H-bonding interactions are indicated by atom numbers and listed under "Bonds". Hydrogen bonds are indicated with dotted lines. R_{H-bond} represents the H-bond distance. Units are in Å. Θ_{H-bond} is the H-bond angle measured in ethylammonium N-H···O (nitrate), 1-AT N-H···O (nitrate), or ethylammonium N-H···N (1-AT). *dd* and *sd* indicate a hydrogen atom in a double donor or a single donor arrangement. *da* and *sa* indicate an oxygen atom in a double acceptor or a single acceptor arrangement. For example, $H_x \cdots O_y$ (*dd*,*da*) represents a H-bond between H_x and O_y where H_x is a hydrogen atom from a double donor, and O_y is an oxygen atom from a double acceptor.

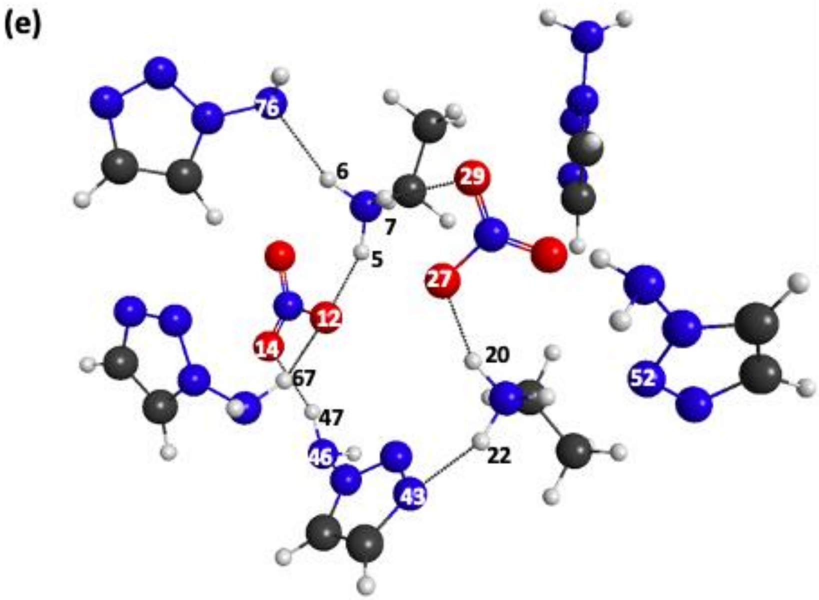

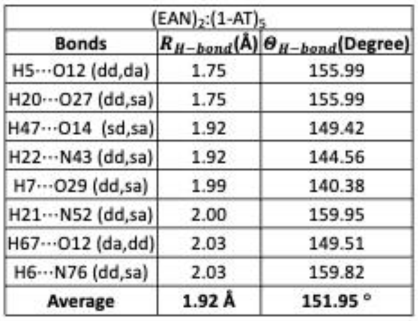

(EAN)$_2$:(1-AT)$_5$		
Bonds	R_{H-bond}(Å)	Θ_{H-bond}(Degree)
H5···O12 (dd,da)	1.75	155.99
H20···O27 (dd,sa)	1.75	155.99
H47···O14 (sd,sa)	1.92	149.42
H22···N43 (dd,sa)	1.92	144.56
H7···O29 (dd,sa)	1.99	140.38
H21···N52 (dd,sa)	2.00	159.95
H67···O12 (da,dd)	2.03	149.51
H6···N76 (dd,sa)	2.03	159.82
Average	**1.92 Å**	**151.95 °**

Figure 11. EFP Optimized geometries for (EAN)$_2$:(1-AT)$_n$ (n=5). Atoms that have H-bonding interactions are indicated by atom numbers and listed under "Bonds". Hydrogen bonds are indicated with dotted lines. R_{H-bond} represents the H-bond distance. Units are in Å. Θ_{H-bond} is the H-bond angle measured in ethylammonium N-H···O (nitrate), 1-AT N-H···O (nitrate), or ethylammonium N-H···N (1-AT). *dd* and *sd* indicate a hydrogen atom in a double donor or a single donor arrangement. *da* and *sa* indicate an oxygen atom in a double acceptor or a single acceptor arrangement. For example, $H_x \cdots O_y$ (*dd,da*) represents a H-bond between H_x and O_y where H_x is a hydrogen atom from a double donor, and O_y is an oxygen atom from a double acceptor.

3.1. Validation of EFP Interaction Energies

The performance of the EFP method has been benchmarked against the RI-MP2 and RI-CCSD(T) methods using the S22[97] and S66[98] data sets for noncovalent interactions and for selected ionic liquids.[4,99,100] Previous calculations have shown that the mean unsigned error (MUE) of EFP interaction energies with respect to coupled-cluster singles, doubles, and perturbative triples in the complete basis set limit [CCSD(T)/CBS] is 0.9 and 0.6 kcal/mol for the S22 and S66 data sets, respectively.[100] The performance of the EFP method for >180 ion pair configurations of ionic liquids demonstrates a similar accuracy relative to the SAPT level of theory. [4,79] In addition, the EFP method can compute interaction energies of strongly H-bonded molecules (e.g. water, formic acid, formamide, and formamidine dimers) to within <2 kcal/mol of the CCSD(T) values.[101] Based on the accuracies of the EFP method relative to the CCSD(T) and SAPT levels of theory, the EFP method is expected to be appropriate for computing accurate interaction energies of strongly H-bonded ionic systems.

To further validate the EFP interaction energies of DeEP species against interaction energies predicted by correlated electronic structure methods, the EFP interaction energies for the $(EAN)_n$ clusters and for the $(EAN)_x$:$(1\text{-}AT)_n$ (x=1,2 and n=1-5) clusters are compared with RI-MP2 and RI-CCSD(T) interaction energies (**Figure 12)**.

The absolute error ($AE_{EFP,ab\ initio}$) is calculated by taking the absolute value of the difference between the EFP interaction energy and the total interaction energy in the *ab initio* method:

$$AE_{EFP,ab\ initio} = \left|E^{EFP}[(EAN)_n] - E^{ab\ initio}[(EAN)_n]\right|. \tag{6}$$

$E^{EFP}[(EAN)_n]$ is the EFP interaction energy and $E^{ab\ initio}[(EAN)_n]$ is the total interaction energy in the *ab initio* method.

The percent error is calculated as:

$$\delta_{ab\ initio}(\%) = \left|\frac{E^{EFP}[(EAN)_n] - E^{ab\ initio}[(EAN)_n]}{E^{ab\ initio}[(EAN)_n]}\right| \times 100 \tag{7}$$

The mean absolute error relative to RI-CCSD(T) is calculated as in Eq. (8) where N is the number of systems.

$$MAE_{EFP,RI-CCSD(T)} = \frac{1}{N}\sum_{s-1}^{N}\left|E^{EFP}[(EAN)_n] - E^{RI-CCSD(T)}[(EAN)_n]\right| \tag{8}$$

To assess the cost-effectiveness of the methods, the total wall clock times (in seconds) of RI-MP2, RI-CCSD(T) and EFP methods is reported in **Table 1**, where it may be seen that the EFP times are orders of magnitude smaller than those for RI-MP2 and RI-CCSD(T). The absolute error, the percent error and the mean absolute error (MAE)[103] of the above methods are reported in **Table 2**.

Table 1. Wall clock time in seconds for EFP, RI-MP2 and RI-CCSD(T) single point energy calculations

Compounds	RI-MP2	RI-CCSD(T)	EFP
$(EAN)_2$	773.7	6,181.4	7.7
$(EAN)_4$	6,296.2	23,102.0	10.0
$(EAN)_6$	13,266.1	184,316.2	14.1
$(EAN)_8$	21,491.2	330,129.1	16.8
$(EAN)_1$:$(1\text{-}AT)_1$	468.5	5,724.3	7.7
$(EAN)_1$:$(1\text{-}AT)_2$	2,335.1	21,973.2	10.4
$(EAN)_1$:$(1\text{-}AT)_3$	5,916.8	283,516.8	9.7
$(EAN)_1$:$(1\text{-}AT)_4$	6,657.4	430,307.6	11.7
$(EAN)_1$:$(1\text{-}AT)_5$	11,179.3	684,648.0	12.0
$(EAN)_2$:$(1\text{-}AT)_1$	3,054.9	22,426.9	8.7
$(EAN)_2$:$(1\text{-}AT)_2$	4,960.2	648,769.9	12.5
$(EAN)_2$:$(1\text{-}AT)_3$	7,127.1	818,239.0	11.6
$(EAN)_2$:$(1\text{-}AT)_4$	10,760.7	1,043,721.1	12.2
$(EAN)_2$:$(1\text{-}AT)_5$	14,067.5	1,309,100.3	12.9

Table 2. Percent errors (δ_{RI-MP2} and $\delta_{RI-CCSD(T)}$), absolute errors ($AE_{EFP,RI-MP2}$ and $AE_{EFP,RI-CCSD(T)}$) and mean absolute errors ($MAE_{EFP,RI-MP2}$ and $MAE_{EFP,RI-CCSD(T)}$) of EFP interaction energies with respect to *ab initio* interaction energies: δ_{RI-MP2} and $\delta_{RI-CCSD(T)}$ are EFP percent errors with respect to RI-MP2 or RI-CCSD(T) interaction energies, respectively computed as in Eq.(6). EFP mean absolute errors (MAE) with respect to RI-MP2 ($MAE_{EFP,RI-MP2}$) or RI-CCSD(T) ($MAE_{EFP,RI-CCSD(T)}$) interaction energies are also listed. The units for MAE are in kcal/mol.

Compounds	$\boldsymbol{\delta_{RI-MP2}}$ **(%)**	$AE_{EFP,RI-MP2}$ **(kcal/mol)**	$MAE_{EFP,RI-MP2}$ **(kcal/mol)**	$\boldsymbol{\delta_{RI-CCSD(T)}}$ **(%)**	$AE_{EFP,RI-CCSD(T)}$ **(kcal/mol)**	$MAE_{EFP,RI-CCSD(T)}$ **(kcal/mol)**
$(EAN)_2$	6.9	3.1	**11.4**	8.3	3.8	**11.5**
$(EAN)_4$	1.9	2.1		8.2	9.7	
$(EAN)_6$	13.2	22.1		4.5	8.8	
$(EAN)_8$	6.5	18.4		8.2	23.5	
$(EAN)_1$:$(1\text{-}AT)_1$	4.0	1.0	**6.4**	3.6	0.9	**5.7**
$(EAN)_1$:$(1\text{-}AT)_2$	9.5	3.7		5.1	1.9	
$(EAN)_1$:$(1\text{-}AT)_3$	10.1	6.2		7.7	4.6	
$(EAN)_1$:$(1\text{-}AT)_4$	13.9	11.3		14.1	11.5	
$(EAN)_1$:$(1\text{-}AT)_5$	10.6	9.9		10.5	9.8	
$(EAN)_2$:$(1\text{-}AT)_1$	18.4	9.9	**7.2**	4.5	3.0	**5.1**
$(EAN)_2$:$(1\text{-}AT)_2$	13.8	8.8		0.6	0.4	
$(EAN)_2$:$(1\text{-}AT)_3$	11.0	8.6		4.2	3.8	
$(EAN)_2$:$(1\text{-}AT)_4$	4.9	4.8		6.8	7.5	
$(EAN)_2$:$(1\text{-}AT)_5$	3.4	3.9		8.8	10.8	
Overall Average	**9.1**		**8.1**	**6.8**		**7.3**

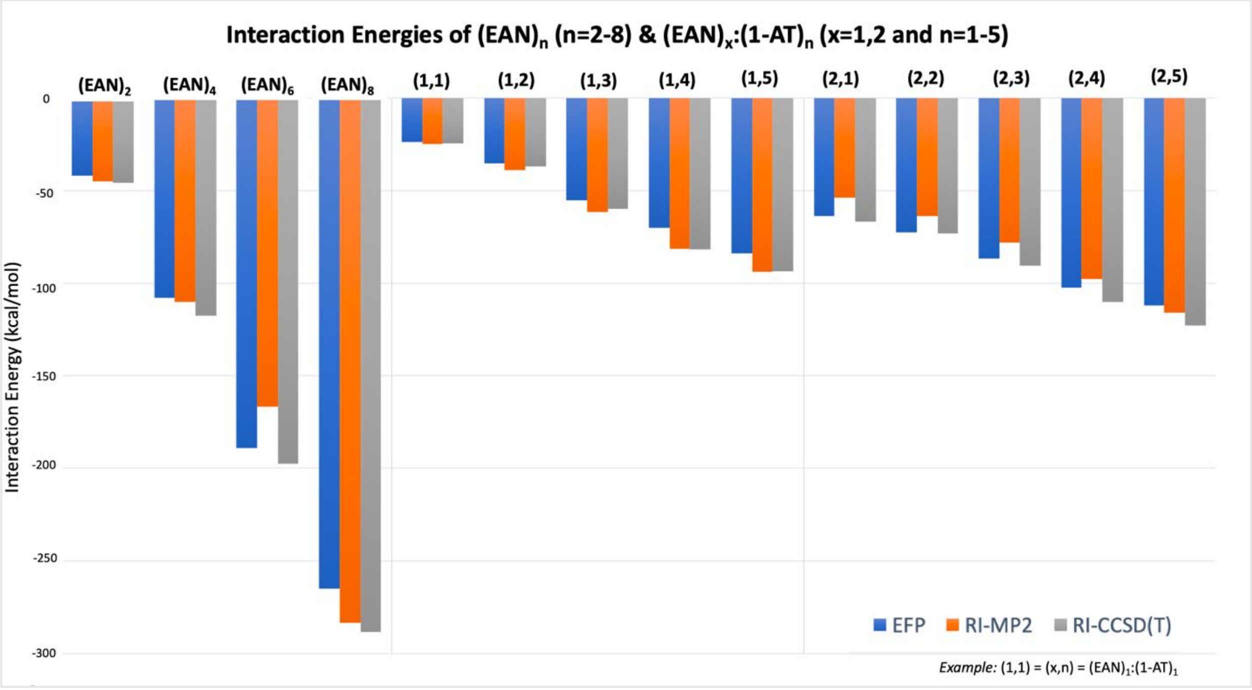

Figure 12. Interaction energies of $(EAN)_n$ IL clusters, $(EAN)_1$:$(1\text{-}AT)_n$, and $(EAN)_2$:$(1\text{-}AT)_n$, for n = 1-5, in kcal/mol. The ratios of $(EAN)_x$:$(1\text{-}AT)_n$ are indicated by labeling them as (*x*,*n*). For example, $(EAN)_2$:$(1\text{-}AT)_1$ is abbreviated as (2,1).

For the EFP-optimized $(EAN)_n$ and $(EAN)_x$:$(1\text{-}AT)_n$ (x=1,2 and n=1-5) clusters, the EFP interaction energies are in reasonable agreement with both *ab initio* methods, especially given the computer time requirements of EFP relative to the two *ab initio* methods. The agreement between EFP and RI-CCSD(T) is slightly better than that with RI-MP2: The average percent error relative to RI-MP2 is 9.1 (The average percent error relative to RI-CCSD(T): 6.8). For example, the $AE_{EFP,RI-CCSD(T)}$ for $(EAN)_1$:$(1\text{-}AT)_1$ is 0.9 kcal/mol, while the EFP wall clock time to compute the single point energy for $(EAN)_1$:$(1\text{-}AT)_1$ is only 7.7 seconds vs 5,724.3 seconds for RI-CCSD(T). As may be seen in **Table 1**, single point EFP interaction energy calculations for the EFP-optimized $(EAN)_n$ and $(EAN)_x$:$(1\text{-}AT)_n$ (x=1,2 and n=1-5) clusters take in the range of 7.7 to 16.8 seconds with an accuracy in reasonable agreement with RI-CCSD(T). Thus, EFP is a computationally effective and accurate method to calculate interaction energies of the IL and DeEP clusters.

For $(EAN)_n$ clusters, the largest $AE_{EFP,RI-MP2}$ and $AE_{EFP,RI-CCSD(T)}$ are 22.1 kcal/mol for $(EAN)_6$ and 23.5 kcal/mol for $(EAN)_8$. The smallest $AE_{EFP,RI-MP2}$ and $AE_{EFP,RI-CCSD(T)}$ are 2.1 kcal/mol for $(EAN)_4$ and 3.8 kcal/mol for $(EAN)_1$. The EFP percent errors with respect to RI-MP2 interaction energies (δ_{RI-MP2}) range from 1.9 to 13.2% and the EFP percent errors with respect to RI-CCSD(T) interaction energies ($\delta_{RI-CCSD(T)}$) range from 4.5 to 8.3% for $(EAN)_2$. The largest δ_{RI-MP2} is associated with $(EAN)_6$. Interestingly, the smallest $\delta_{RI-CCSD(T)}$ is also associated with $(EAN)_6$. The mean absolute errors of EFP interaction energies for $(EAN)_n$ with respect to RI-MP2 or RI-CCSD(T) interaction energies are 11.4 kcal/mol and 11.5 kcal/mol respectively.

For $(EAN)_1$:$(1\text{-}AT)_n$ (n=1-5) clusters, the largest $AE_{EFP,RI-MP2}$ and $AE_{EFP,RI-CCSD(T)}$ are, respectively, 11.3 kcal/mol and 11.5 kcal/mol both for $(EAN)_1$:$(1\text{-}AT)_4$. The smallest $AE_{EFP,RI-MP2}$ and $AE_{EFP,RI-CCSD(T)}$ are ~1 kcal/mol for $(EAN)_1$:$(1\text{-}AT)_1$. δ_{RI-MP2} ranges from 4.0 to 13.9% and $\delta_{RI-CCSD(T)}$ ranges from 3.6 to 14.1%. The MAE of the EFP interaction energy with respect to RI-CCSD(T) is 5.7 kcal/mol, slightly smaller than the MAE with respect to RI-MP2 (6.4 kcal/mol). Therefore, overall the EFP method predicts interaction energies for the $(EAN)_1$:$(1\text{-}AT)_n$ clusters that are in reasonable agreement with the CCSD(T) level of theory, with an error less than 6 kcal/mol on average.

For the $(EAN)_2$:$(1\text{-}AT)_n$ (n=1-5) clusters, the largest $AE_{EFP,RI-MP2}$ is 9.9 kcal/mol for the $(EAN)_2$:$(1\text{-}AT)_1$ and the error decreases as the size of the cluster increases. On the other hand, $AE_{EFP,RI-CCSD(T)}$ generally increases as the size of the cluster increases from 3.0 kcal/mol to 10.8 kcal/mol, except for $(EAN)_2$:$(1\text{-}AT)_2$ with an error of only 0.4 kcal/mol. The MAE of the EFP interaction energy with respect to RI-CCSD(T) for the $(EAN)_2$:$(1\text{-}AT)_n$ (n=1-5) clusters is 5.1

kcal/mol, indicating that the EFP interaction energies with respect to the RI-CCSD(T) values agree better than with RI-MP2 (MAE=7.2 kcal/mol).

Overall, for the EFP optimized $(EAN)_n$ and $(EAN)_x$:(1-AT)$_n$ (x=1,2 and n=1-5) clusters, the EFP interaction energies have smaller MAEs relative to RI-CCSD(T) than relative to the RI-MP2 interaction energies. Therefore, EFP can compute $(EAN)_n$ and $(EAN)_x$:(1-AT)$_n$ (x=1,2 and n=1-5) interaction energies in reasonable agreement with the RI-CCSD(T) interaction energies with orders of magnitude less computing time than required for the corresponding RI-CCSD(T) calculation. It is concluded that EFP geometry optimizations starting from the lowest energy structures obtained from EFP-MC global optimizations is a reasonable method to predict interaction energies of $(EAN)_n$ and $(EAN)_x$:(1-AT)$_n$ (x=1,2 and n=1-5) DeEP clusters.

3.2. EFP Interaction Energy Components and Geometries

Studies of the nature of intermolecular interactions in ILs has mainly been focused on Coulomb forces since ILs are comprised of ions.[1,2,3] Other fundamental interactions such as dispersion, polarization, exchange-repulsion and charge transfer have been largely overlooked due to the strong Coulombic interactions. However, extensive *ab initio* based intermolecular interaction studies by Gordon[4,103], Hunt[47,104], Izgorodina[105,106], Kirchner[107,108], Tsuzuki[109,110], and others[111,112,113,114] have suggested that contributions from other fundamental interactions to the energetics of ionic liquid systems can be important. In the following paragraphs, the EFP interaction energies are decomposed into their components (See Eq. (1)).

3.2.1. $(EAN)_n$ IL clusters

The EFP interaction energies for the $(EAN)_n$ (n=2-16) clusters, as well as the percentage of the total EFP interaction energy for each EFP component (e.g. Coulomb, exchange-repulsion, polarization, dispersion and charge transfer) are analyzed here in order to provide an understanding of intermolecular interactions, in the absence of the hydrogen bonding species 1-AT. The EFP interaction energies and the percent of the total EFP interaction energy for each EFP components are reported in **Figure 13**.

EFP Interaction Energy $(EAN)_n$ IL clusters:

As the size of $(EAN)_n$ IL clusters increases, the Coulomb interaction becomes stronger (e.g. more negative); the attractive Coulomb interaction increases from -47.7 kcal/mol to -590.4 kcal/mol as the cluster size increase from $(EAN)_2$ to $(EAN)_{16}$. As shown in the bottom section of Figure 15, the Coulomb interaction contributes 104 to 113 % percent of the total EFP energies. These percentages are greater than 100% because the exchange repulsion contribution is opposite in sign. Due to the ionic nature of the systems being studied, the Coulomb term is expected to be the leading contribution to the intermolecular interaction energy.[47] However, the percent contribution of the Coulomb term to the total EFP interaction stays fairly constant as n increases. Indeed, there is little change in the percent contributions to the total EFP interaction energy for any of the EFP components.

The polarization interaction increases from -15.2 to -118.8 kcal/mol as the cluster size increases. Polarization, which accounts for the intramolecular charge redistribution in response to the external electric field[49,50,51] of other molecules (fragments), increases as the size of the cluster increases; for example, a significant polarization contribution is expected in $(EAN)_n$ IL clusters and their H-bond networks. In the H-bonded systems, polarization can contribute up to 20% of the total intermolecular interaction energy.[52] In the present case, the polarization energy accounts for 21 to 28% of the overall EFP interaction energies in $(EAN)_n$ IL clusters due to the dipole-induced dipole interactions between EAN monomers.[105,116,117,118]

The magnitude of the dispersion interaction increases from -14.7 to -217.1 kcal/mol as the size of the $(EAN)_n$ cluster increases to n=16. Dispersion comprises 29-39% to the total interaction energies in each cluster, slightly more than the polarization contribution. Since dispersion arises from the interaction between induced multipoles[50,51,100], the dispersion interaction is an important factor for the overall interactions in ion pairs. Dispersion interactions increase between ion pairs with increasing cluster size.

The exchange-repulsion becomes more positive as the size of the cluster increases, contributing -66 to -74% of the total interaction energies in each cluster. Because the exchange-repulsion represents the destabilization of the total interactions, negative signs are used for the percentages. The EFP CT interaction is the smallest contribution to the total interaction energies for $(EAN)_n$ IL clusters, amounting to 7-9 % on average. The CT interactions increase in magnitude as the cluster size increases.

As previously discussed, in H-bond networks of protic ILs[1,2,3,4,47,105,106,111], strong long-range interactions are a primary driving force of H-bond network formation[2,3,4,47]. Of course, increases in short-range interactions such as exchange-repulsion balances the attractive Coulomb and dispersion interactions. Although CT interactions make the smallest contribution to the total EAN interaction energies, CT does stabilize the cluster.

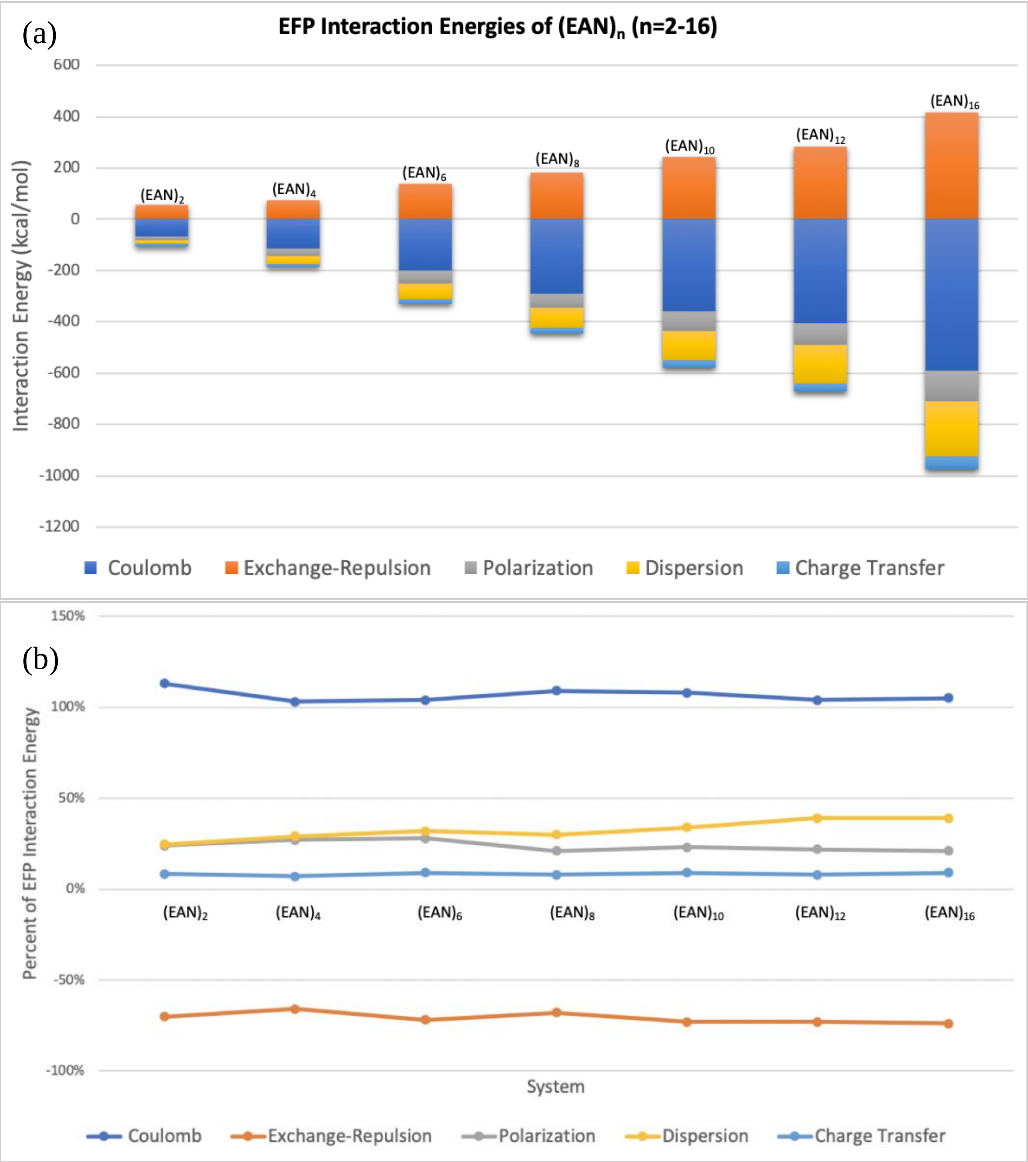

Figure 13. EFP interaction energies (a) and energy decomposition for EAN clusters in percent contribution (b). A negative entry in the percent contribution indicates a repulsive contribution.

As the EAN cluster size increases, the larger clusters begin to resemble the bulk. The percentage contribution of each EFP interaction energy appears to converge. In particular, as the EAN cluster size increases, the Coulomb, polarization, dispersion, charge transfer interaction and exchange repulsion contributions seem to converge to 105%, 20%, 40%, 9% and -74% of the total EFP interaction energy, respectively.

Geometries for *$(EAN)_n$ IL clusters:*

The intermolecular interactions in the $(EAN)_n$ IL clusters **(Figure 2 to 7)** are reflected in the H-bond networks in the EFP-optimized geometries. The average H-bond distances increase as the number of EAN monomers in the clusters increases. The average X-H---Y H-bond angles (X = N,O) for $(EAN)_n$ ($n \geq 2$) range from 141.9° to 153.5°, which are smaller than the H-bond angle of 155.6° in the EAN monomer. Smaller angles between H-bond donors lead to larger dipole-dipole and dipole-induced dipole interactions resulting in longer H-bond distances.[47] Likewise, the H-bond distances for $(EAN)_n$ ($n \geq 2$) range from 1.77 to 1.83 Å, which are longer than the H-bond distance in the EAN monomer (1.75Å).

Hydrogen bonds in ILs are dominated by long-range interactions. However, the CT interaction can play an important role as a stabilizing energy term.[31] CT is commonly present in complex H-bond networks; the CT contribution can change as H-bond geometries change.[47,] In H-bond networks, CT interactions contribute to cooperative and anti-cooperative effects in H-bonds[30,31,32,119,120]. These effects are associated with H-bond formation by double donors (DD) and double acceptors (DA) defined in Section 2.5. As one might expect, the number of DD and DA arrangements increases as the cluster size increases, leading to more cooperative and anti-cooperative effects in the $(EAN)_n$ H-bond networks.

The number of DDs and DAs are reported in **Table 3.** The total number of DDs and DAs increases from 2 to 18 as the size of cluster increases from $(EAN)_2$ to $(EAN)_{16}$.

The total number of DDs and DAs for $(EAN)_n$ (n=10,12) is 14 with eight DDs and six DAs in the clusters. Additional EAN monomers added to $(EAN)_{10}$ act as single donors

(SDs) or single acceptors (SAs) and have H-bond interactions with DDs and DAs. Such H-bond interactions between SDs and DAs or DDs and SAs stabilize geometries and contribute to energy lowering effects that arise from CT interactions.[30,33] In addition, the H-bonds with DDs and DAs act as building blocks for extensive H-bond networks in EAN clusters.

Table 3. Number of double donors and double acceptors in $(EAN)_n$ (n=2-16).

	$(EAN)_2$	**$(EAN)_4$**	**$(EAN)_6$**	**$(EAN)_8$**	**$(EAN)_{10}$**	**$(EAN)_{12}$**	**$(EAN)_{16}$**
# of DD	1	3	4	6	8	8	10
# of DA	1	1	2	6	6	6	8
Total (DD+DA)	2	4	6	12	14	14	18

In $(EAN)_n$ clusters, H-bond networks associated with DAs and DDs form enclosed cyclic structures or loop-like structures (open-end, not quite cyclic) in various sizes.

$(EAN)_2$ forms a cyclic structure between the two EAN monomers, shown in **Figure 2**. This cyclic $(EAN)_2$ structure consists of an ethylammonium N-H···O (nitrate) hydrogen bond associated with one DD ([EA]-N4) and one DA (O27-(nitrate)): N4-H5···O12, N4-H6···O27, N19-H20···O27 and N19-H20···O15 H-bond moieties comprise the cyclic configuration. $(EAN)_2$ is the smallest EAN cluster that forms an H-bond network associated with a DD and a DA.

$(EAN)_4$ forms a (not quite cyclic) loop structure (**Figure 3**) consisting of three DDs ([EA]-N19, [EA]-N49 and [EA]-N34) closed as shown in the optimized structure of $(EAN)_2$. Each DD has two ethylammonium N-H···O (nitrate) hydrogen bond moieties which build extended H-bond chains consisting of O···H-N-H···O. H20 and H21 are hydrogen atoms bonded to N19 and associated with an extended H-bond chain, O27···H20-N19-H21···O12. O12 forms a H-bond with H5 of $[EA]^+$ cation, which can extend the H-bond network further. $(EAN)_6$ forms an S-shaped loop structure consisting of four DDs ([EA]-N19, [EA]-N49, [EA]-N79, and [EA]-N34) and two DAs (O12-, O57-(nitrate)).

The optimized geometries of the larger $(EAN)_n$ clusters (n=8-16) are composed of closed-loop (cyclic) structures and loop structures that are nearly cyclic. $(EAN)_8$ forms a single cyclic structure (**Figure 4**) with five EA DDs (N49, N64, N94, N109 and N79) and four nitrate-based DAs O27, O72, O87 and O57. Chains of H-bonds are also formed; for example, by [EA]-N49 with a single acceptor O42-(nitrate) and [EA]-N19 with O27-(nitrate). $(EAN)_{10}$ (**Figure 4**), forms two cyclic structures, one with three EA DDs (N49, N4, N19) and two nitrate DAs (O12-and O27). The second ring structure is also formed with three EA DDs (N49, N79, and N64) and three nitrate DAs (O87, O57, and O27).

$(EAN)_{12}$ is composed of two separate cyclic structures (**Figure 5**) and an open-loop structure similar to the one shown in $(EAN)_4$. $(EAN)_{16}$ has the largest number of DDs and DAs (10 and 8, respectively), and therefore, it can form the most extended H-bond network. $(EAN)_{16}$ consists of one linear chain with four EAN monomers and one open-loop structure with 12 EAN monomers: The linear H-bond chain is constructed with three DDs (N229, N119, and N169) and three DAs (O207, O177, O147). DDs and DAs excluding those participating in the H-bond chain are components of the acyclic loop structure.

Extended loop structures and cyclic structures in large $(EAN)_n$ (n>6) clusters are built by intermolecular interactions, which are provided by long-range interactions and energy stabilizing effects of CT in surrounding EAN monomers. The observed H-bonds appear to be a common structural motif in $(EAN)_n$ clusters and can be considered as evidence for the three-dimensional H-bond network character of the H-bonds in bulk EAN.

3.2.2. $(EAN)_1$:$(1\text{-}AT)_n$ (n=1-5)

The effects of one to five 1-AT molecules on the EAN monomer are explored by examining EFP interaction energies and comparing them with those of $(EAN)_n$. Since (EAN):(1-AT)~~$_n$~~ mixtures are prepared by mixing the $(EAN)_n$ IL and 1-AT neutral hydrogen bond donor, examining the intermolecular interactions between 1-AT and the EAN monomer is important. The ratio between the EAN monomer and 1-AT is varied in order to examine the interaction energy change that may occur from the interactions between 1-AT molecules.

EFP Interaction Energy for $(EAN)_1$:$(1\text{-}AT)_n$ (n=1-5) clusters:

The EFP interaction energies for the $(EAN)_1$:$(1\text{-}AT)_n$ (n=1-5) DeEP clusters as well as the percentage contribution of each EFP interaction energy component to the total EFP energy are reported in **Figure 14**.

Due to the ionic nature of the DeEP, EFP Coulomb interactions are still the leading contribution to the total EFP interaction energies. The percent contribution of the Coulomb interaction ranges from 101 % to 117 % for n=1 – 5.

For n=1, the percent contributions of the Coulomb and dispersion interactions are 117 % and 37 % respectively. For n=2, the percent contribution of the Coulomb interaction decreases from 117 % to 101 %, while the dispersion contribution increases from 37 % to 60 %. However, as more 1-AT molecules are added to the system (e.g. when n=3 – 5), the percent contribution of Coulomb interaction is fairly constant at 110 –

115 %. The percent contribution of dispersion for n=3 – 5 is also fairly constant at 50 to 56 %.

Recall that in the set of $(EAN)_n$ IL clusters, the dispersion contribution ranges from 25 – 39 %. In comparison, the dispersion interaction accounts for 50 - 60 % of the total interactions for $(EAN)_1$:$(1\text{-}AT)_n$ when n=2 – 5. Increasing the number of 1-AT molecules increases the percent contribution of the dispersion interactions. The dispersion interaction in $(EAN)_1$:$(1\text{-}AT)_n$ increases likely due to the π- π interactions between the electron-rich triazole rings in the 1-AT molecules.[115]

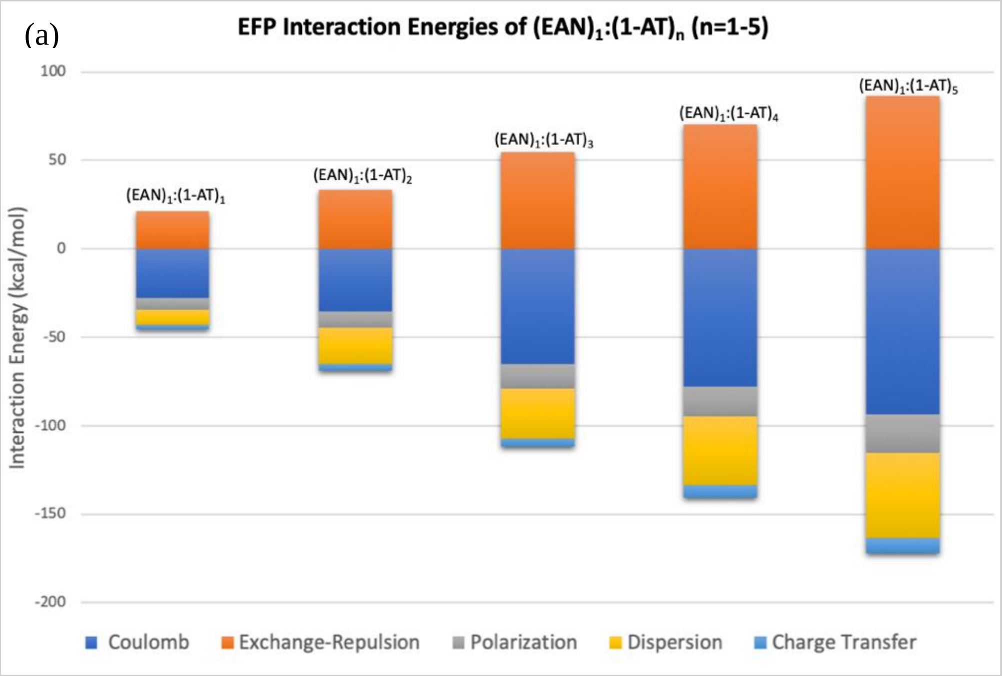

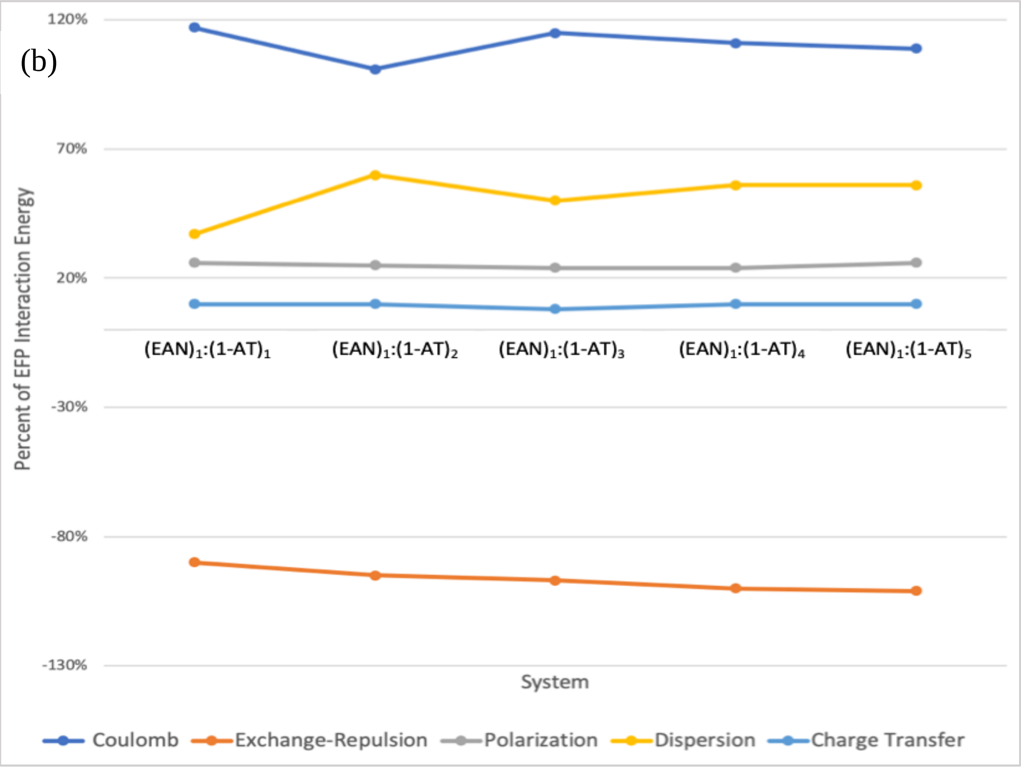

Figure 14. EFP interaction energies (a) and energy decomposition for $(EAN)_1:(1\text{-}AT)_n$ DeEP in percent composition (b). A negative entry indicates a repulsive contribution.

The percent contribution of the polarization interaction ranges between 24-26% of the total EFP interaction energy in $(EAN)_1:(1\text{-}AT)_n$, and this contribution is fairly constant as *n* increases.

The percent contribution of the exchange-repulsion interaction becomes larger in magnitude as *n* increases, from -90% for n=1 to -101% for *n*=5, indicating stronger destabilization effects as *n* increases. The CT interaction is the smallest contribution to the total interaction energies in the $(EAN)_1:(1\text{-}AT)_n$ DeEP clusters. The CT interaction percent contribution is fairly constant for the values of n, ranging from 8 to 10 % of the total EFP interaction energy.

Considering the percent contribution of the long-range interactions (Coulomb, dispersion and polarization) in the $(EAN)_1:(1\text{-}AT)_n$, clusters, there are stronger dispersion interaction contributions in $(EAN)_1$:$(1\text{-}AT)_n$ than in pure $(EAN)_n$ ILs due to the presence of the 1-AT molecules.

Noticeable trends in the changes in the percent contributions of short-range interactions are illustrated by the exchange-repulsion interaction. As n increases, the percent contribution of the exchange-repulsion increases, indicating that the increase in the number of 1-AT molecules is responsible for the increase in the destabilization effect of the total interaction energies.

As observed for the EAN clusters, the EFP Coulomb, polarization, dispersion and charge transfer interaction energy contributions appear to converge and may resemble the "bulk" medium. In particular, the Coulomb, polarization, dispersion and charge transfer interaction contributions converge to 108%, 26%, 56% and 10% of the total EFP energy, respectively.

Geometries for $(EAN)_1$:$(1\text{-}AT)_n$ (n=1-5) clusters:

The EFP-optimized geometries of $(EAN)_1$:$(1\text{-}AT)_n$ (n=1-5) clusters and their H-bond networks are displayed in **Figure 6** to **Figure 8.** The average H-bond distances in $(EAN)_1$:$(1\text{-}AT)_n$ (n=1-5) range from 1.96 Å to 1.98 Å. The average H-bond distances in $(EAN)_1$:$(1\text{-}AT)_n$ can be separated into two types of H-bonds: The average internal EAN H-bond distances are 1.70 Å and the average H-bond distances between EAN and 1-AT are 1.93 Å. The average H-bonds between EAN and 1-AT are longer than the average H-bonds between $[EA]^+$ and $[NO_3]^-$ because the H-bonds in deep eutectic mixtures are dominated by the Coulomb and dispersion interactions mainly between hydrogen bond donors and acceptors.[13,14,15,17,18] Therefore, it is expected that there are H-bond networks formed between the EAN monomer and 1-AT in the $(EAN)_1$:$(1\text{-}AT)_n$ clusters.

The H-bond geometries are examined here as *n* increases in the cluster. The EFP-optimized structures for $(EAN)_1$:$(1\text{-}AT)_n$ show that the number of H-bond interactions between 1-AT molecules and EAN monomers increase as n increases. Interestingly, 1-AT can participate in H-bonds as a hydrogen bond donor and as an acceptor simultaneously. For example, the EFP-optimized structure of $(EAN)_1$:$(1\text{-}AT)_1$ in **Figure 6a** shows how the 1-AT molecule interacts with the EAN monomer to form H-bonds as a H-bond donor: hydrogen atom H22 on 1-AT forms a H-bond with O12 in $[NO_3]^-$, and simultaneously N17 in 1-AT accepts H5 from $[EA]^+$ and forms H-bonds.

The optimized geometry of $(EAN)_1$:$(1\text{-}AT)_2$ in **Figure 6b** shows that each 1-AT molecule has a H-bond interaction with the EAN monomer: H32 and O14 form a H-bond. The nitrogen atom (N18) from the 1-AT ring accepts a hydrogen (H6) from $[EA]^+$ to form a H-bond. The H-bond interactions between a neutral H-bond donor and an ionic species are sometimes viewed as a formation of a “bulky ion” in a deep eutectic solvent mixture. The bulky ion is responsible for lowering lattice energies and for exhibiting a liquid phase at a room temperature.[10,13,14,15]

The EFP-optimized structure of the $(EAN)_1$:$(1\text{-}AT)_3$ cluster in **Figure 7c** shows that all three 1-AT molecules are involved in H-bond interactions. A H-bond between H5 and O12-(nitrate) occurs in the EAN monomer. A H-bond interaction between H22-(1-AT) and O12-(nitrate) forms a “bulky anion”. Here, O12-(nitrate) serves as a DA. The number of DDs and DAs in $(EAN)_1$:$(1\text{-}AT)_n$ are listed in **Table 4**. The DDs and DAs are also identified and listed in the table.

Interestingly, H-bond interactions between two 1-AT molecules are also observed. H42-(1-AT) is a H-bond donor and N18-(1-AT) is a H-bond acceptor. The H-bond interaction between two 1-AT molecules can be driven by dispersion interactions. According to the H-bond analysis done by Peschel and coworkers[121] using *ab initio* molecular dynamics with the GTH-BLYP functional, intermolecular H-bonds between two 1,2,3-triazole molecules with π- π interactions were observed under specific conditions: Two triazole molecules were arranged in a (parallel) sandwich configuration to maximize the π- π interactions with a distance between the two centers of mass of 3.7 to 5 Å[121]. The intermolecular H-bond was formed between a hydrogen atom (bonded to a nitrogen atom on the hetero aromatic ring) on one 1,2,3-triazole and a nitrogen atom in the aromatic ring on the other 1,2,3-triazole. The resulting intermolecular H-bond distance was reported as 2.5 – 2.75 Å. The observation in the current work that dispersion can play an important role in the EFP interaction energies is consistent with the work of Peschel *et al*.

The (1-AT)-H42 and N18-(1-AT) can also form a H-bond via π - π interactions. Those two 1-AT molecules, (1-AT)-H42 and N18-(1-AT), are in a parallel configuration. The distance between the two centers of mass of the two 1-AT molecules is 4.34Å, which falls in the distance range reported by Peschel and coworkers[121]. The resulting H-bond H42···N18 distance is 2.09Å, in good agreement with the dispersion driven intermolecular H-bonds observed in a previous study.[121]

The EFP-optimized structure of $(EAN)_1$:$(1\text{-AT})_4$ (**Figure 7d**) shows that three 1-AT molecules form H-bonds with the EAN monomer, while the fourth 1-AT molecule does not have an H-bond interaction with the other molecules in the cluster. In addition, there is an extended H-bond network that is partly constructed from DDs and DAs. Two 1-AT molecules are H-bond donors (H22 and H33) and form H-bonds with a double acceptor, O12-(nitrate). N48-(1-AT) is a H-bond acceptor that has an H-bond interaction with H6. H6 is a hydrogen atom bonded to a DD, [EA]-N4. [EA]-N4 has two hydrogen atoms, H6 and H5, which have H-bond interactions with two H-bond acceptors (O12 and N48). The H-bond interactions with DDs and DAs makes extensive H-bond networks that connect three 1-AT molecules and the EAN monomer. As shown for the $(EAN)_n$ IL clusters, the CT interaction associated with DDs and DAs can play an important role as a stabilizing energy term and also form an energetically stable geometry.

In the EFP-optimized structure of $(EAN)_1$:$(1\text{-}AT)_5$ (**Figure 8**) four 1-AT molecules form H-bond interactions and one 1-AT does not form any significant H-bond interactions with the EAN monomer nor with the other 1-AT molecules. H42, H22, H33 from 1-AT molecules participate in H-bonds. N48-(1-AT) acts as a H-bond acceptor.

H-bonds with a DD and a DA are also observed in the optimized geometry of the $(EAN)_1$:$(1\text{-}AT)_5$ cluster. The double acceptor, O12-(nitrate), forms H-bond interactions with H22-(1-AT) and H6-$[EA]^+$. The double donor, $[EA]^+$-N4 donates H5 to form a H-bond with O12-(nitrate) and also donates H6 to form a H-bond with N48-(1-AT). Extended H-bond networks with a DD and DA are formed between the EAN monomer and 1-AT molecules.

Based on the EFP interaction energy analysis, long-range interactions like Coulomb and dispersion contribute to the H-bond networks in $(EAN)_1$:$(1\text{-}AT)_n$. However, considering the H-bond interactions with DDs and DAs, the energy stabilizing effects of CT in surrounding EAN monomers and 1-AT molecules are also important. As *n* increases, the number of H-bond interactions between EAN and 1-AT increase. The bulky ion geometries appear to be a common structural motif in $(EAN)_1$:$(1\text{-}AT)_n$ clusters, and H-bond structures between 1-AT molecules form H-bond networks that are likely to extend to larger clusters and in the bulk.

Table 4. Number of double donor and double acceptor in $(EAN)_1$:$(1\text{-}AT)_x$ (x=1-5).

	$(EAN)_1$:$(1\text{-}AT)_1$	**$(EAN)_1$:$(1\text{-}AT)_2$**	**$(EAN)_1$:$(1\text{-}AT)_3$**	**$(EAN)_1$:$(1\text{-}AT)_4$**	**$(EAN)_1$:$(1\text{-}AT)_5$**
# of DD	0	1	0	1	1
# of DA	1	0	1	1	1
Total (DD+DA)	1	1	1	2	2
DD	-	[EA]-N4	-	[EA]-N4	[EA]-N4
DA	O12-(nitrate)	-	O12-(nitrate)	O12-(nitrate)	O12-(nitrate)

3.2.3. EFP interaction energy of $(EAN)_2$:$(1\text{-}AT)_n$ (n=1-5)

The effects of one to five 1-AT molecules on the EAN dimer are explored by examining EFP interaction energies and comparing them with those of $(EAN)_2$. The effect of 1-AT molecules on EAN dimers can be directly compared to the EFP interaction energies of the EAN dimer itself discussed in Section 3.2.1. The EFP interaction energies for the $(EAN)_2$:$(1\text{-}AT)_n$ clusters as well as the percent composition of each EFP interaction energy with respect to the total EFP energy are reported in **Figure 15** and discussed in the following subsection.

EFP Interaction Energy for $(EAN)_2$:$(1\text{-}AT)_n$ (n=1-5) clusters:

The percent contribution of the Coulomb interaction in $(EAN)_2$:$(1\text{-}AT)_n$ (n=1-5) is in the range 102 – 109 % of the total EFP interaction energy, fairly constant relative to the value of n. This is only slightly smaller than the percent contribution of Coulomb interactions in EAN dimer (113 %).

The percent contribution of the polarization energy in $(EAN)_2$:$(1\text{-}AT)_n$ decreases from 29% to 22% of the total EFP interaction energy relative to EAN dimer: The exchange-repulsion in $(EAN)_2$:$(1\text{-}AT)_n$ accounts for -70 to -97% of the total interaction energy. Negative signs are used here to represent the destabilization of the total interaction. The percent contribution of exchange-repulsion in the EAN dimer is -70%, so the addition of one 1-AT molecule to EAN dimer does not increase the exchange-repulsion percent contribution. However, when n=2 – 5, the percent contribution of exchange-repulsion increases from -77 to -97 %. The exchange-repulsion energy for n=3 is -97% and exhibits greater destabilization than when n=4,5 for which the exchange-repulsion interactions account for ~-80% of the total energy.

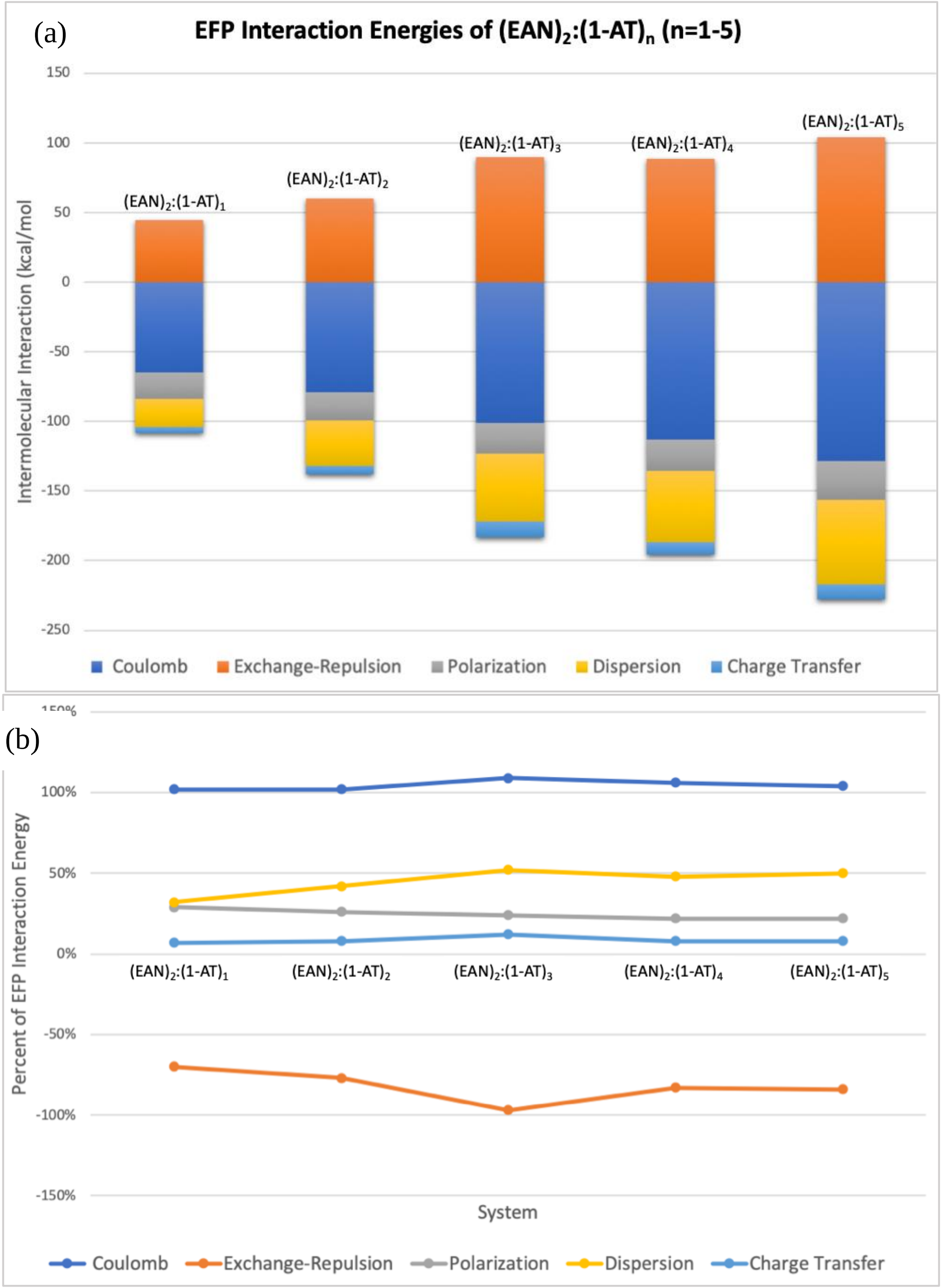

Figure 15. EFP interaction energies (kcal/mol) (a) and energy decomposition (percent composition)(b) for $(EAN)_2$:$(1\text{-}AT)_n$. A negative entry in part (b) indicates a repulsive contribution.

The CT interaction is the smallest contribution to the total interaction energy in the $(EAN)_2$:$(1\text{-}AT)_n$ DeEP clusters, in the range 7-12 %. This is slightly larger than that in EAN dimer.

Geometries for (EAN)$_2$:(1-AT)$_n$ (n=1-5) clusters:

The EFP-optimized geometries of (EAN)$_2$:(1-AT)$_n$ (n=1-5) clusters and their H-bond networks are displayed in **Figures 9** to **11.** The average H-bond distances in (EAN)$_2$:(1-AT)$_n$ (n=1-5) range from 1.92 to 2.01 Å with average H-bond angles of 142.6 to 152.0 °. More specifically, the average H-bond distances of internal EAN are 1.75 Å. The average H-bond distances between EAN and 1-AT are 2.00 Å.

The average H-bond distances and angles are similar to those of the (EAN)$_1$:(1-AT)$_n$ clusters. However, the (EAN)$_2$:(1-AT)$_n$ (n=1-5) clusters have longer average H-bond lengths and wider H-bond angles than the EAN dimer (1.78 Å and 141.9° respectively).

As for the (EAN)$_1$:(1-AT)$_n$ clusters, Coulomb and dispersion interactions are the dominant interactions for forming H-bonds between H-bond donors and acceptors in (EAN)$_2$:(1-AT)$_n$ clusters. However, the CT interactions involved in H-bond formation via DDs and DAs can stabilize the cluster geometries and total interaction energies of the cluster. The total numbers of DDs and DAs in (EAN)$_2$:(1-AT)$_n$ (n=1-5) clusters are listed in **Table 5**. DDs and DAs are identified and listed in the table. As shown in the table, there are no changes in the total number of DDs and DAs as n increases. N4 and N19 serve as DDs and O12 is a DA throughout the clusters.

Table 5. Number of double donor and double acceptor in (EAN)$_2$:(1-AT)$_n$ (n=1-5).

	(EAN)$_2$:(1-AT)$_1$	**(EAN)$_2$:(1-AT)$_2$**	**(EAN)$_2$:(1-AT)$_3$**	**(EAN)$_2$:(1-AT)$_4$**	**(EAN)$_2$:(1-AT)$_5$**
# of DD	2	2	2	2	2
# of DA	1	1	1	1	1
Total (DD+DA)	3	3	3	3	3
DD	[EA]-N4 [EA]-N19	[EA]-N4 [EA]-N19	[EA]-N4 [EA]-N19	[EA]-N4 [EA]-N19	[EA]-N4 [EA]-N19
DA	O12-(nitrate)	O12-(nitrate)	O12-(nitrate)	O12-(nitrate)	O12-(nitrate)

The EFP-optimized structure of $(EAN)_2$:$(1\text{-}AT)_1$ shows that a hydrogen atom (H22) from $[EA]^+$ is donated to N33 on the N-N bond side of the aromatic ring (**Figure 9a**) creating a cyclic configuration. The H-bond networks associated with DD (N19) and DA (O12) comprise a closed loop. The CT interactions involving H-bonds with DD and DA also have an energy lowering effect and make the cluster energetically stable.

$(EAN)_2$:$(1\text{-}AT)_2$ forms a closed loop similar to that observed in $(EAN)_2$:$(1\text{-}AT)_1$. The additional 1-AT molecule is located outside of the closed loop (**Figure 9b)**. The cyclic H-bond structure is constructed with DDs (N19 and N4) and one DA (O12). The 1-AT outside of the closed loop does not participate in H-bond interactions with other molecules.

A similar cyclic configuration to that in $(EAN)_2$:$(1\text{-}AT)_2$ appears in the optimized structures of $(EAN)_2$:$(1\text{-}AT)_3$ (in **Figure 10c**). Two 1-AT molecules outside of the closed loop structure in $(EAN)_2$:$(1\text{-}AT)_3$ geometry do not involve H-bond interactions with molecules that form the closed loop H-bond structure.

Unlike the H-bond interactions shown in $(EAN)_2$:$(1\text{-}AT)_{3,}$ 1-AT molecules outside of the closed loop in $(EAN)_2$:$(1\text{-}AT)_n$ (n=4,5) do participate in H-bonding interactions with EAN monomers in the closed loop. For example, in $(EAN)_2$:$(1\text{-}AT)_4$ (**Figure 10d**), there is a H-bond interaction between (1-AT)-N62 and H6-$[EA]^+$. (1-AT)-H67 and O15-(nitrate) also form a H-bond. (1-AT)-N62 acts as a H-bond acceptor, while (1-AT)-H67 behaves as a H-bond donor. In $(EAN)_2$:$(1\text{-}AT)_5$ (**Figure 11.**), H-bond interactions (1-AT)-N76 and H6-$[EA]^+$, (1-AT)-H67 and O12-(nitrate), and (1-AT)-N52 and H21-$[EA]^+$ are observed. (1-AT)-N76 and (1-AT)-N52 are H-bond acceptors, while (1-AT)-H67 is a

H-bond donor. In both $(EAN)_2$:$(1\text{-}AT)_4$ and $(EAN)_2$:$(1\text{-}AT)_5$, 1-AT can act as H-bond donor and acceptor.

The extended closed loop structures in $(EAN)_2$:$(1\text{-}AT)_n$ clusters are built by intermolecular interactions provided by long-range interactions plus the energy stabilizing effects of CT. This interesting closed loop H-bond appears to be a common structural motif in $(EAN)_2$:$(1\text{-}AT)_n$ clusters. Additional 1-AT molecules interact with the closed loop H-bond structure and build H-bonds external to the loop. This stable closed loop H-bond structure can be considered as evidence for a three-dimensional H-bond network character of the H-Bonds in larger $(EAN)_2$:$(1\text{-}AT)_n$ DeEP clusters.

For $(EAN)_2$:$(1\text{-}AT)_n$ (n=1-5), the EFP Coulomb, polarization, dispersion and charge transfer interaction energy contributions converge to 109%, 26%, 56% and 10% of the total EFP energy respectively. The exchange-repulsion interaction contribution is -101%. These percentages are similar to those of $(EAN)_1$:$(1\text{-}AT)_n$ (n=1-5). This suggests that there are no significant differences in the interaction energies between EAN monomer and 1-AT compared to the interaction between EAN dimer and 1-AT complexes as the cluster sizes increase.

3.3. Three-Center Four-Electron (3C-4E) interactions in EAN

The QUAOs in the EAN monomer are analyzed to assess whether the QUAO orbitals participating in the H-bonding interactions are three-center four-electron (3C-4E) interactions as has been suggested in previous QUAO analyses of hydrogen bonding.[33,122] The orbital occupations (Occ) of corresponding atoms are shown in parentheses in **Figure 16**.

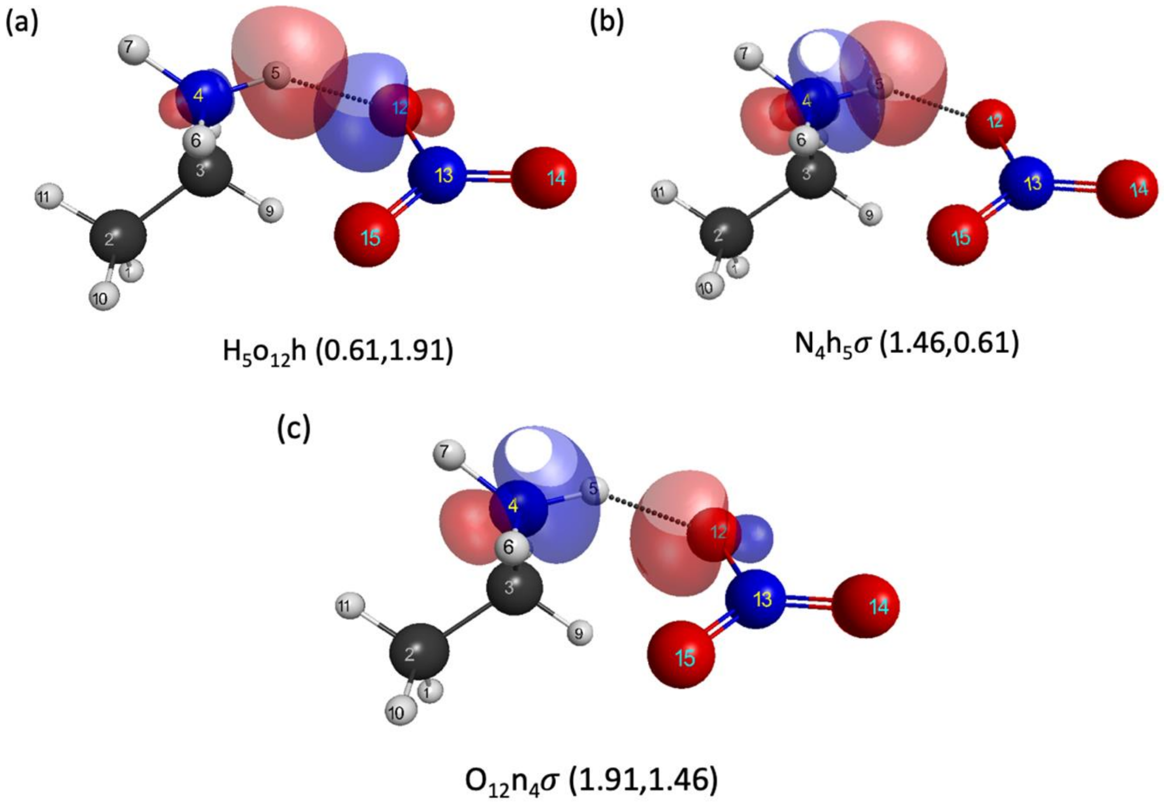

$H_5o_{12}h$ (0.61,1.91)

$N_4h_5\sigma$ (1.46,0.61)

$O_{12}n_4\sigma$ (1.91,1.46)

Figure 16. Qualitatively unique QUAOs for the $H_5o_{12}h$ H-bonding interaction in the EAN monomer. The bond labels and occupations for each QUAO are shown. The atom numbering system follows Figure 2a. (a) QUAOs involved in a hydrogen bond between hydrogen (H5) and oxygen atom (O12) (b) QUAOS involved in a sigma bond between nitrogen atom (N4) and hydrogen atom (H5) (c) QUAOs for oxygen-nitrogen interactions.

The occupation of N4 in $N_4h_5\sigma$ in **Figure 16b** is 1.46, and that of H5 is 0.61. Because the occupation of a lone pair on the oxygen atom is ~1.91, the electron-rich lone pair QUAO on O12 acts as a nucleophile.[123] The lone pair QUAO on O12 ($O_{12}pl$) interacts with a QUAO centered on the hydrogen atom (H5), whose occupation is 0.61. The sum of the three orbital occupations for three centers participating in the H-bond interactions is 3.98 electrons, so these three atoms can be said to form a three-center four-electron (3C-4C) interaction. Similar analyses apply to the other hydrogen bonds in the clusters studied in this work. Hereafter, any of the significant intermolecular H-bonds (BO > 0.10) in the $(EAN)_n$ IL clusters will be referred to as 3C-4E interactions.[124,125,126]

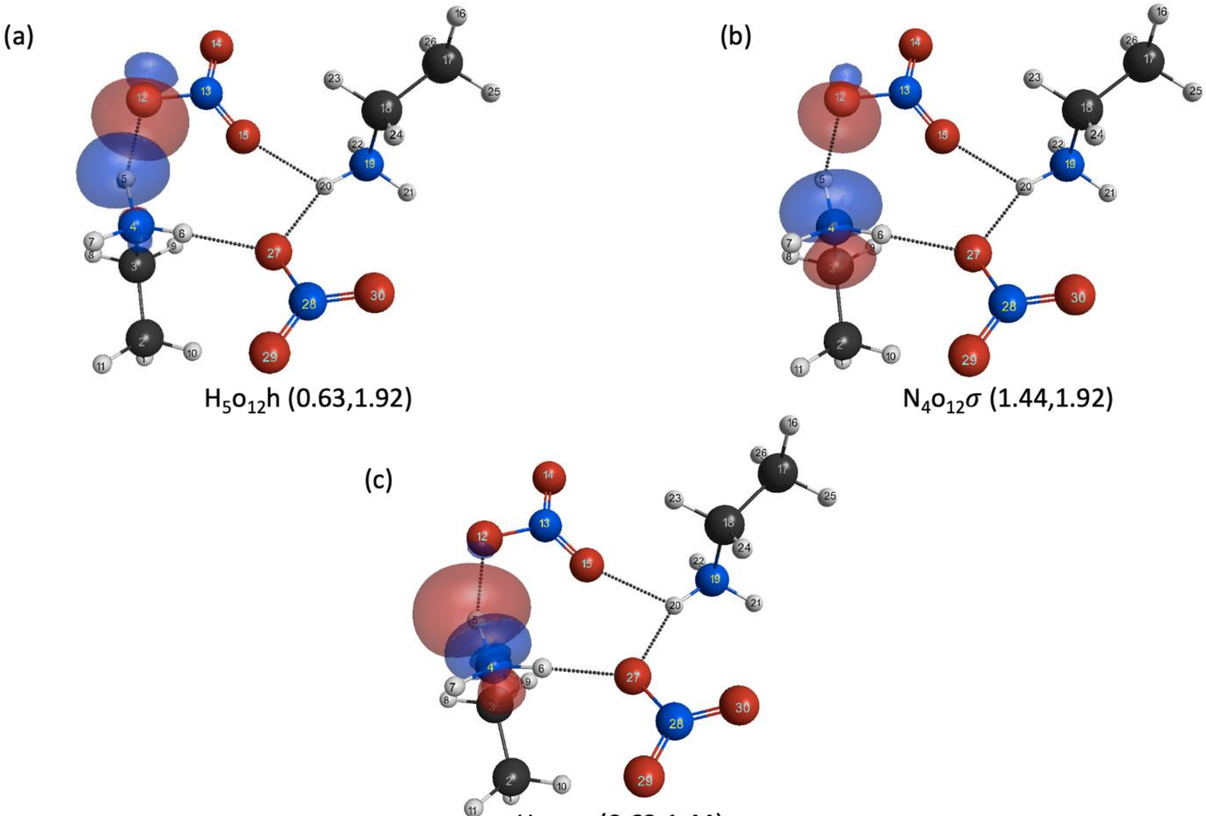

$H_5o_{12}h$ (0.63,1.92)

$N_4o_{12}\sigma$ (1.44,1.92)

$H_5n_4\ \sigma$ (0.63,1.44)

Figure 17. Qualitatively unique QUAOs for the EAN dimer. The bond labels and occupations for each QUAO are shown. The atom numbering system follows Figure 2b. (a) QUAOs involved in a hydrogen bond between hydrogen (H5) and oxygen atom (O12) (b) QUAOS involved in a σ bond between nitrogen atom (N4) and hydrogen atom (H5) (c) QUAOs for oxygen-nitrogen interactions.

The QUAOs in the EAN dimer are analyzed in the same way that the QUAO in the EAN monomer was assessed; the QUAOs in the EAN dimer are examined to determine whether the QUAO orbitals participating in the H-bonding interactions are the 3C-4E interactions as observed in the QUAOs of the EAN monomer. The occupation of N4 in $N_4h_5\sigma$ in **Figure 17b** is 1.44, and that of H5 is 0.63. The occupation of a lone pair on the oxygen atom is 1.92. The lone pair QUAO on O12 ($O_{12}pl$) interacts with a QUAO centered on the hydrogen atom (H5), whose occupation is 0.61. The sum of the occupations for N4, H5 and O12 for the EAN dimer is 3.98 electrons supporting the conclusion that the H-bonding interaction in the EAN dimer is a 3C-4E interaction.

3.4. Three-Center Four-Electron (3C-4E) interactions in $(EAN)_x$:$(1\text{-}AT)_n$ DeEP clusters

The QUAOs in the $(EAN)_x$:$(1\text{-}AT)_n$ are analyzed to assess whether the QUAO orbitals participating in the H-bonding interactions are 3C-4E interactions as are the QUAOs for the H-bonds in $(EAN)_n$ clusters. The H-bonding interactions in the $(EAN)_x$:$(1\text{-}AT)_n$ may be categorized into four different cases depending on which molecules are forming H-bonding interactions - $[EA]^+$:$[NO3]^-$ within an EAN molecule, $[NO3]^-$:1-AT, 1-AT:1-AT, and $[EA]^+$:1-AT. As an example, **Figure 18** shows the QUAOs in $(EAN)_1$:$(1\text{-}AT)_3$ that are participating in H-bonding interactions: Figure 20(a) to (c) represent the H-bonds between $[NO3]^-$ and the 1-AT molecule. The occupation of H32 is 0.69. The lone pair QUAO on O15 has an occupation of 1.91 and N31 which forms a σ bond with H32 has an occupation of 1.34. The sum of occupations for H32, N31 and O15 is 3.94 electrons. Figure 20(d) to (f) are the QUAOs for the H-bonding interaction between $[EA]^+$:$[NO3]^-$ within an EAN molecule. The occupations of H5, lone pair oxygen O12 and N4 in $N_4h_5\sigma$ are 0.62, 1.92 and 1.44 respectively. The sum of these three orbital occupations is 3.98 electrons. Figure 20(g) through (i) are the QUAOs for the H-bonding interactions between 1-AT molecules. The nitrogen lone pair on the triazole ring (N18) is acting as an H-bond acceptor, and H42 covalently bonded to N41 on the other 1-AT molecule is an H-bond donor. The orbital occupations for N18, H42 and N41 are 1.93, 0.70 and 1.44. The sum of these three orbital occupations is 3.97.

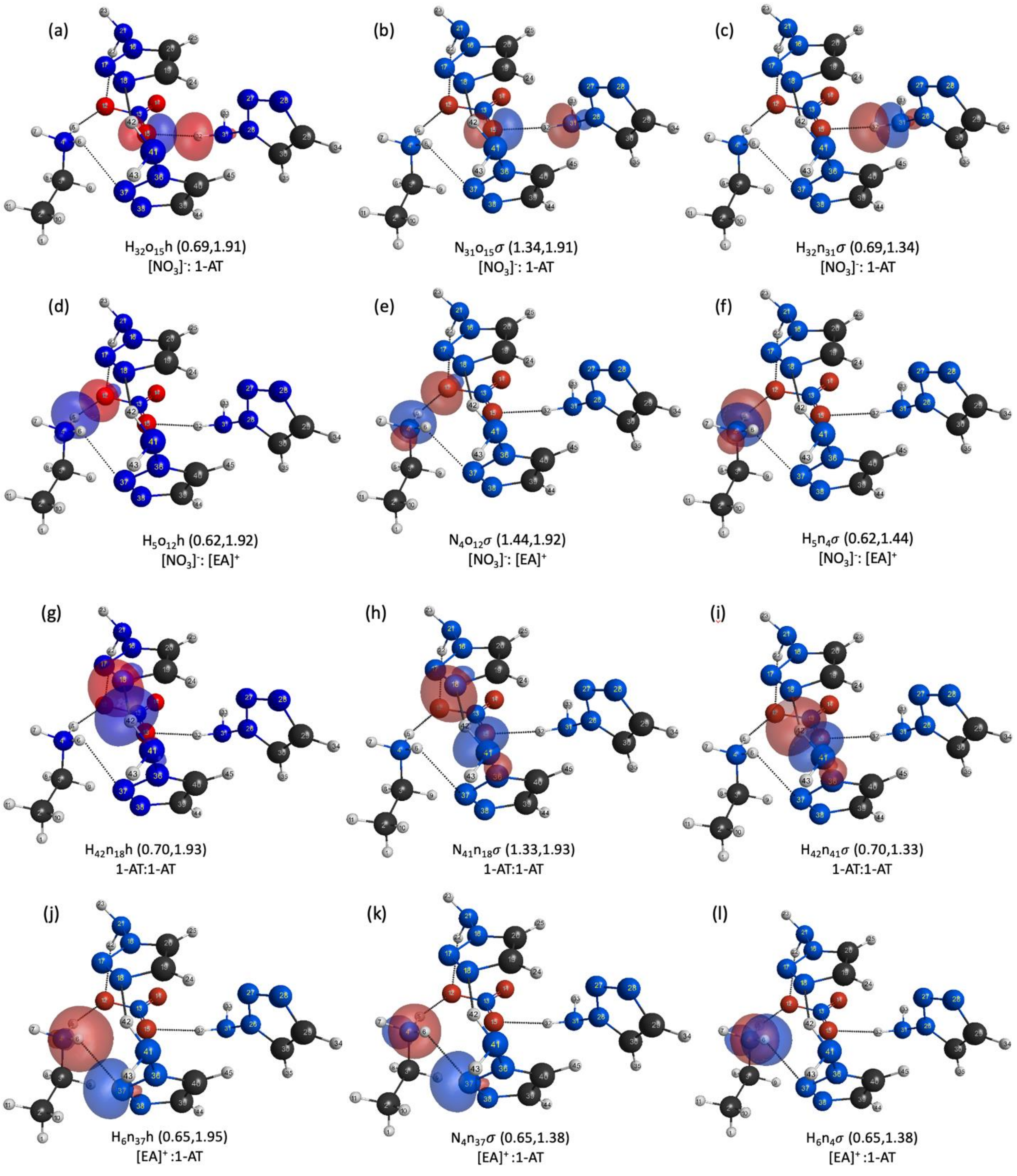

$H_{32}o_{15}h$ (0.69,1.91)
$[NO_3]^-$: 1-AT

$N_{31}o_{15}\sigma$ (1.34,1.91)
$[NO_3]^-$: 1-AT

$H_{32}n_{31}\sigma$ (0.69,1.34)
$[NO_3]^-$: 1-AT

$H_5o_{12}h$ (0.62,1.92)
$[NO_3]^-$: $[EA]^+$

$N_4o_{12}\sigma$ (1.44,1.92)
$[NO_3]^-$: $[EA]^+$

$H_5n_4\sigma$ (0.62,1.44)
$[NO_3]^-$: $[EA]^+$

$H_{42}n_{18}h$ (0.70,1.93)
1-AT:1-AT

$N_{41}n_{18}\sigma$ (1.33,1.93)
1-AT:1-AT

$H_{42}n_{41}\sigma$ (0.70,1.33)
1-AT:1-AT

$H_6n_{37}h$ (0.65,1.95)
$[EA]^+$:1-AT

$N_4n_{37}\sigma$ (0.65,1.38)
$[EA]^+$:1-AT

$H_6n_4\sigma$ (0.65,1.38)
$[EA]^+$:1-AT

Figure 18. Qualitatively unique QUAOs for $(EAN)_1$:$(1\text{-}AT)_3$. The bond labels and occupations for each QUAO are shown. The atom numbering system follows Figure 7c. (a) through (c) represent QUAOs in H-bonding interactions between $[NO_3]^-$:1-AT. (d) through (f) are QUAOs of H-bonding interactions between $[NO_3]^-$:1-AT. (g) through (i) are QUAOs of H-bonding interactions in 1-AT:1-AT, and (j) to (l) are the H-bonding interacting QUAOs in $[EA]^+$ and 1-AT.

Lastly, Figure 20(j) through (l) are the QUAOs corresponding to H-bonding interactions in $[EA]^+$:1-AT. The nitrogen lone pair in the triazole ring (N37) on 1-AT is an H-bond acceptor, and H6 from $[EA]^+$ forms an H-bond with N37 as the QUAOs for $H_6n_{37}h$ in Figure 20(j) shows. The N-N interaction occurs between N37 and N4. The orbital occupations for N37, H6 and N4 are 1.95, 0.65 and 1.38 respectively, and the sum of these three orbital occupations is 3.98 electrons. As the sum of orbital occupations of the three atoms engaging in H-bonding interactions in the above four examples in $(EAN)_x$:$(1\text{-}AT)_n$ are ~4 electrons, the H-bonding interactions observed in $(EAN)_x$:$(1\text{-}AT)_n$ are 3C-4E interactions for all four types of H-bonding interactions (*e.g.* $[EA]^+$:$[NO3]^-$, $[NO3]^-$:1-AT, 1-AT:1-AT, and $[EA]^+$:1-AT).

3.5. KBO Bonding analysis of $(EAN)_n$ clusters

The kinetic bond orders (KBOs) are calculated using the QUAOs for the H-bonds in $(EAN)_n$ clusters in order to provide an understanding of these H-bonds associated with DDs and DAs, in the absence of the hydrogen bonding species 1-AT. KBOs for bonding interactions are generally negative. Therefore, the convention used here is that KBOs become stronger when the values become more negative.

Considering that the H-bonding interaction in the EAN monomer is the 3C-4E interaction between N, H, and O, it is reasonable to include the interaction between H-bond donor nitrogen in $[EA]^+$ and H-bond acceptor oxygen in $[NO_3]^-$ (N···O interaction) as part of the overall H-bonding (H···O) interaction energy. The KBO analysis of the N···O interactions shows that the N···O bonding interaction strengthens the H-bonding in the EAN clusters. For example, the H-bonding interaction in the EAN monomer (**Figure 2a**) between the QUAO on O12 (occ=1.91) and the QUAO on N4 (occ=1.46) has a KBO=-1.9 kcal/mol. Then the KBO of N4···O12 may be added to the KBO of the $H_5o_{12}h$ interaction (KBO=-5.7 kcal/mol) in order to fully assess the bonding interaction between the three centers. The KBO of $H_5 o_{12} h$ including the N4···O12 contribution is -7.5 kcal/mol.

The average KBOs and BOs of the H-bonds in the $(EAN)_1$ through $(EAN)_{16}$ are listed in **Table 6**. The average KBOs of H-bonds including the corresponding N ··· O interaction are given in parentheses.

Table 6. Average bond orders (BO) and KBOs (kcal/mol) for H-bonds in $(EAN)_n$ IL clusters. R_{H-bond} represents the H-bond distance in Å. The number of double donors (DDs), double acceptors (DAs) are also listed in the table. The KBOs in parentheses are the sums of the H-bond and N···O KBOs.

	$(EAN)_1$	**$(EAN)_2$**	**$(EAN)_4$**	**$(EAN)_6$**	**$(EAN)_8$**	**$(EAN)_{10}$**	**$(EAN)_{12}$**	**$(EAN)_{16}$**
KBO (kcal/mol)	-5.7 (-7.5)	-4.3 (-5.7)	-4.0 (-5.4)	-3.9 (-5.2)	-3.8 (-5.2)	-3.8 (-5.1)	-3.8 (-5.1)	-3.7 (-4.9)
BO	0.33	0.27	0.26	0.25	0.25	0.25	0.24	0.24
R_{H-bond} (Å)	1.75	1.77	1.77	1.79	1.82	1.81	1.83	1.82
# of DD	0	1	3	4	6	8	8	10
# of DA	0	1	1	2	6	6	6	8

As the size of the cluster increases from $(EAN)_1$ to $(EAN)_{16}$, the average KBO weakens from -5.7 to -3.7 kcal/mol and the average magnitude of the BO decreases from 0.33 to 0.24. In addition, the QUAO analysis of the $(EAN)_n$ clusters suggests that larger $(EAN)_n$ clusters are associated with a higher number of DDs and DAs. This trend indicates that the strengths of the H-bonds decrease with the increase in size of the EAN clusters and the concomitant increase in the number of DDs and DAs in the clusters. Referred to as “sacrificial bonding”,[127] the electron density of the H-bond participating atoms is spread over multiple bonds, and consequently those bonds become weaker on average.[33] It is evident that the strengths of the H-bonds weaken as more DDs and/or DAs are in the clusters.

3.6. KBO Bonding analysis of $(EAN)_1$:$(1\text{-}AT)_n$ (n =1 – 5)

The effects of one to five 1-AT molecules on the EAN monomer are explored by examining the H-bonding interactions based on the QUAO and KBOs. The average bond orders (BO) and KBOs (kcal/mol) of the H-bonds between EAN monomer and 1-AT in $(EAN)_1$:$(1\text{-}AT)_n$ (n=1-5) are listed in **Table 7**.

The QUAO bonding analysis of $(EAN)_1$:$(1\text{-}AT)_n$ DeEP clusters suggests that as *n* increases, the average magnitudes of the BOs decrease and the H-bond lengths increase. The average magnitude of the BOs decreases from 0.33 to 0.20 and the average KBOs for the H-bonds also weakens from -5.7 to -2.5 kcal/mol. The H-bond distances increase from 1.75 to 2.02 Å as *n* increases.

Table 7. Average bond orders (BO) and KBOs (kcal/mol) of the H-bonds between EAN monomer and 1-AT in $(EAN)_1$:$(1\text{-}AT)_n$ (n=1-5). H-bond distances (R) are in Å. The KBO in parentheses is the sum of the KBO of the H-bond and $N\cdots O$ and $N\cdots N$ KBOs.

EAN:1-AT			
System	**BO**	**KBO (kcal/mol)**	**R(Å)**
$(EAN)_1$	0.33	-5.67 (-7.55)	1.75
$(EAN)_1$:$(1\text{-}AT)_1$	0.24	-2.71 (-3.83)	1.86
$(EAN)_1$:$(1\text{-}AT)_2$	0.22	-2.67 (-3.72)	2.00
$(EAN)_1$:$(1\text{-}AT)_3$	0.21	-2.54 (-3.83)	2.00
$(EAN)_1$:$(1\text{-}AT)_4$	0.20	-2.51 (-3.81)	2.02
$(EAN)_1$:$(1\text{-}AT)_5$	0.20	-2.52 (-3.82)	2.02

However, it is important to recognize that there are four different types of hydrogen bonding: $[EA]^+$:$[NO3]^-$ within an EAN molecule, $[NO3]^-$:1-AT, 1-AT:1-AT, and $[EA]^+$:1-AT. The averaged H-bond interactions in $(EAN)_1$:$(1\text{-}AT)_n$ are separated into the four types in **Table 8**.

Table 8. Average bond orders (BO), KBOs (kcal/mol) for H-bonds in $(EAN)_1$:$(1\text{-}AT)_n$ (n=1-5). R represents the H-bond distance in Å. H-bonding interactions in $(EAN)_1$:$(1\text{-}AT)_n$ are further categorized in Table 8A - $[EA]^+$: $[NO_3]^-$, Table 8B - $[NO3]^-$:1-AT, Table 8C - $[EA]^+$: 1-AT and Table 8D - 1-AT:1-AT. Occ(H), Occ(O) and Occ(N) represent occupations of the QUAO centered on H, O and N, respectively. For the H-bonding interactions in $[EA]^+$: $[NO_3]^-$ and $[NO3]^-$:1-AT, the KBOs in parenthesis is the sum of the H-bond and N···O KBOs. For the H-bonding interactions in $[EA]^+$: 1-AT, the KBOs in parenthesis is the sum of the H-bond $N \cdots N$ KBOs.

A. $[EA]^+$: $[NO_3]^-$					
System	**BO**	**KBO (kcal/mol)**	**R(Å)**	**Occ(H)**	**Occ(O)**
$(EAN)_1$:$(1\text{-}AT)_1$	0.30	-5.11 (-6.77)	1.75	0.61	1.91
$(EAN)_1$:$(1\text{-}AT)_2$	0.30	-5.13 (-6.83)	1.75	0.62	1.92
$(EAN)_1$:$(1\text{-}AT)_3$	0.30	-5.06 (-6.73)	1.75	0.62	1.92
$(EAN)_1$:$(1\text{-}AT)_4$	0.27	-4.60 (-6.12)	1.75	0.63	1.93
$(EAN)_1$:$(1\text{-}AT)_5$	0.27	-4.63 (-6.14)	1.75	0.63	1.93
B. $[NO3]^-$:1-AT					
System	**BO**	**KBO (kcal/mol)**	**R(Å)**	**Occ(H)**	**Occ(O)**
$(EAN)_1$:$(1\text{-}AT)_1$	0.18	-1.91 (-2.72)	2.02	0.61	1.92
$(EAN)_1$:$(1\text{-}AT)_2$	0.16	-1.77 (-2.41)	1.98	0.69	1.90
$(EAN)_1$:$(1\text{-}AT)_3$	0.15	-1.44 (-1.91)	2.04	0.69	1.94
$(EAN)_1$:$(1\text{-}AT)_4$	0.14	-1.18 (-1.70)	2.05	0.69	1.96
$(EAN)_1$:$(1\text{-}AT)_5$	0.12	-0.92 (-1.30)	2.09	0.69	1.96
C. $[EA]^+$: 1-AT					
System	**BO**	**KBO (kcal/mol)**	**R(Å)**	**Occ(H)**	**Occ(N)**
$(EAN)_1$:$(1\text{-}AT)_1$	0.11	-0.69 (-1.06)	2.17	0.61	1.96
$(EAN)_1$:$(1\text{-}AT)_2$	0.15	-0.98 (-1.40)	2.22	0.65	1.94
$(EAN)_1$:$(1\text{-}AT)_4$	0.19	-2.28 (-3.04)	2.02	0.64	1.91
$(EAN)_1$:$(1\text{-}AT)_5$	0.29	-4.11 (-5.57)	1.86	0.66	1.90
D. 1-AT:1-AT					
System	**BO**	**KBO (kcal/mol)**	**R(Å)**	**Occ(H)**	**Occ N)**
$(EAN)_1$:$(1\text{-}AT)_2$	0.08	-0.65 (-1.00)	2.20	0.61	1.97
$(EAN)_1$:$(1\text{-}AT)_3$	0.19	-1.67 (-2.38)	2.09	0.70	1.93
$(EAN)_1$:$(1\text{-}AT)_4$	0.10	-1.00 (-1.30)	2.19	0.62	1.98
$(EAN)_1$:$(1\text{-}AT)_5$	0.11	-1.14 (-1.50)	2.18	0.70	1.93

Table 8A shows that the strength of the internal EAN $[EA]^+$:$[NO3]^-$ H-bond, as measured by the KBO values, decreases slightly as the number of 1-AT molecules present increases from 1 to 5. As may be seen in **Tables 8B** and **8D**, the hydrogen bond KBOs between both EA^+ and NO_3^- are much smaller than those within EAN, thereby decreasing the overall average KBOs considerably. The H-bond KBOs between two 1-AT molecules (**Table 8C**) are also small. So, the large decrease in H-bond KBOs upon adding a 1-AT molecule is mostly due to the H-bonds that involve 1-AT and only slightly due to the decrease in H-bond strengths within the EAN molecule. Overall, the H-bond strengths decrease in the order $[EA]^+$:$[NO_3]^-$ >>$[EA]^+$:1-AT>$[NO_3]^-$:1-AT

3.7. KBO Bonding analysis of $(EAN)_2$:$(1\text{-}AT)_n$ (n=1-5)

As summarized in **Tables 9 and 10**, a similar interpretation applies to the impact of adding 1 to 5 1-AT molecules to the EAN dimer. Atoms participating in bonding interactions, bond orders (BO), KBOs (kcal/mol) for the H-bonds in $(EAN)_2$:$(1\text{-}AT)_n$ (n=1-5) are listed in Supplementary Information, **Table S5.4.**

Adding 1-AT molecules to the EAN dimer decreases the average H-bond KBO due to interactions with 1-AT molecules, as was noted above for the EAN monomer, for the same reasons. The average H-bond KBO of EAN dimer is -4.3 kcal/mol. The average H-bond KBO of $(EAN)_2$:$(1\text{-}AT)_1$ decreases to -2.5 kcal/mol. The average H-bond KBOs of $(EAN)_2$:$(1\text{-}AT)_2$ to $(EAN)_2$:$(1\text{-}AT)_5$ only change minimally ranging from -2.5 kcal/mol to -2.3 kcal/mol. The weakest H-bond KBOs are observed in $(EAN)_2$:$(1\text{-}AT)_3$, with an average H-bond KBO of 2.2 kcal/mol.

Table 9. Average bond orders (BO) and KBOs (kcal/mol) for H-bonds in $(EAN)_2$:$(1\text{-}AT)_n$ (n=1-5). R represents the H-bond distance in Å. The KBO in parentheses is the sum of H-bond, N ⋯ O and N ⋯ N KBOs.

EAN:1-AT			
System	**BO**	**KBO (kcal/mol)**	**R(Å)**
$(EAN)_2$	0.27	-4.27 (-5.71)	1.77
$(EAN)_2$:$(1\text{-}AT)_1$	0.23	-2.51 (-3.73)	1.96
$(EAN)_2$:$(1\text{-}AT)_2$	0.22	-2.47 (-3.62)	2.05
$(EAN)_2$:$(1\text{-}AT)_3$	0.21	-2.24 (-3.44)	2.08
$(EAN)_2$:$(1\text{-}AT)_4$	0.21	-2.25 (-3.45)	2.10
$(EAN)_2$:$(1\text{-}AT)_5$	0.22	-2.30 (-3.52)	2.10

Table 10. Average bond orders (BO), KBOs (kcal/mol) for H-bonds in (EAN)$_2$:(1-AT)$_n$ (n=1-5). R represents the H-bond distance in Å. H-bonding interactions in (EAN)$_2$:(1-AT)$_n$ are further categorized in Table 10A - [EA]$^+$: [NO$_3$]$^-$, Table 10B - [NO3]$^-$:1-AT, and Table 10C - [EA]$^+$: 1-AT. Occ(H), Occ(O) and Occ(N) represent occupations of the QUAO centered on H, O and N, respectively. For the H-bonding interactions in [EA]$^+$: [NO$_3$]$^-$ and [NO3]$^-$:1-AT, the KBOs in parenthesis is the sum of the H-bond and N···O. For the H-bonding interactions in [EA]$^+$: 1-AT, the KBOs in parenthesis is the sum of the H-bond N ··· N KBOs.

A. [EA]$^+$: [NO$_3$]$^-$

System	BO	KBO (kcal/mol)	R (Å)	Occ(H)	Occ(O)
(EAN)$_2$:(1-AT)$_1$	0.29	-5.02 (-6.65)	1.75	0.65	1.98
(EAN)$_2$:(1-AT)$_2$	0.29	-5.0 (-6.63)	1.75	0.66	1.97
(EAN)$_2$:(1-AT)$_3$	0.29	-4.86 (-6.42)	1.76	0.66	1.97
(EAN)$_2$:(1-AT)$_4$	0.28	-4.77 (-6.39)	1.78	0.66	1.98
(EAN)$_2$:(1-AT)$_5$	0.28	-4.70 (-6.34)	1.78	0.66	1.97

B. [NO3]$^-$:1-AT

System	BO	KBO (kcal/mol)	R (Å)	Occ(H)	Occ(O)
(EAN)$_2$:(1-AT)$_1$	0.14	-1.17 (-1.80)	2.17	0.68	1.97
(EAN)$_2$:(1-AT)$_2$	0.13	-1.20 (-1.71)	2.17	0.68	1.97
(EAN)$_2$:(1-AT)$_3$	0.15	-1.32 (-1.88)	2.15	0.68	1.97
(EAN)$_2$:(1-AT)$_4$	0.15	-1.41 (-2.02)	2.14	0.68	1.97
(EAN)$_2$:(1-AT)$_5$	0.14	-1.45 (-2.02)	1.98	0.69	1.94

C. [EA]$^+$: 1-AT

System	BO	KBO (kcal/mol)	R (Å)	Occ(H)	Occ(N)
(EAN)$_2$:(1-AT)$_1$	0.15	-1.03 (-1.48)	2.13	0.66	1.94
(EAN)$_2$:(1-AT)$_2$	0.16	-1.28 (-1.79)	2.09	0.68	1.94
(EAN)$_2$:(1-AT)$_3$	0.14	-1.25 (-1.76)	2.17	0.66	1.94
(EAN)$_2$:(1-AT)$_4$	0.18	-1.73 (-2.42)	2.10	0.67	1.94
(EAN)$_2$:(1-AT)$_5$	0.24	-2.84 (-3.71)	1.98	0.66	1.93

4. Conclusion

It was shown that the EFP method estimates the interaction energies of the (EAN)$_n$ IL and (EAN)$_x$:(1-AT)$_n$ DeEP clusters with an accuracy that is similar to the interaction energies calculated by RI-CCSD(T) but at a small fraction of the computational cost. Along with the intermolecular interaction energy calculations using EFP, the intermolecular interactions and the H-bond formations in ethyl ammonium nitrate (EAN) and 1-amino-1,2,3 triazole (1-AT)-based DeEP have been studied using the QUAO bonding analysis.

The interaction energies, geometries, and H-bond interactions in (EAN)$_n$ IL clusters have been studied in order to understand the intermolecular interactions occurring between EAN monomers, in the absence of the hydrogen bonding species 1-AT. For $(EAN)_n$ IL clusters, the Coulomb interaction is the leading contribution in $(EAN)_n$ clusters followed by dispersion interactions. Long-range interactions are significant for modeling $(EAN)_n$ IL accurately but short-range interactions such as exchange-repulsion and CT are also important. The CT interaction is the smallest contribution to the $(EAN)_n$ IL (n=2-16) clusters. However, CT is an energy lowering component of the total interaction energies for the formation of intermolecular H-bonds between EAN monomers.

Intermolecular H-bonds of the $(EAN)_n$ IL clusters are analyzed using the QUAO and KBO analyses based on the EFP-optimized geometries. Since H-bond interactions are 3C-4E interactions, the N···O bonding interactions should be included in the analysis. The QUAO and KBO analyses suggest that the H-bond interactions associated with DDs and DAs in $(EAN)_n$ clusters have weaker H-bonding strengths because the electron density of the H-bond participating atoms is spread over multiple bonds, and those bonds become weaker on average.

The interaction energies, geometries, and H-bond interactions in $(EAN)_1$:$(1\text{-}AT)_n$ (n=1-5) DeEP clusters show that the percent contribution of the Coulomb interaction varies slightly as *n* increases but stays fairly constant as a leading interaction term. As the number of 1-AT molecules increases, the contribution of the dispersion interaction increases, due to the π- π interactions between the electron-rich aromatic ring of the 1-AT molecules. H-bonding interactions with 1-AT molecules are produced mainly by dispersion. Short-range interactions also change as the number of 1-AT molecules increases. As *n* increases, the exchange-repulsion contribution increases. The CT interaction is the smallest contribution and stays constant at ~10 % as n increases. However, this is 1-2 % higher than that in the pure (EAN)n clusters, suggesting that 1-AT can increase the CT interaction contributions to the total EFP interaction energy.

As the cluster get larger, the interaction energies of both EAN clusters and EAN:1-AT clusters converge to what might be their values in the "bulk".

The interaction energies, geometries, and H-bond interactions in $(EAN)_2$:$(1\text{-}AT)_n$ (n=1-5) DeEP clusters have been computed and are compared with the EAN dimer. An increase in the number of 1-AT molecules interacting with the EAN dimer can lower the contributions of the Coulomb and polarization interactions, and increase the contributions of the dispersion interactions. For short-range interactions, the increase in the number of 1-AT molecules in the cluster can have higher destabilization effects via an increase in the exchange-repulsion interaction. However, CT interactions stay fairly constant.

The QUAO and KBO analysis of $(EAN)_x$:$(1\text{-}AT)_n$ DeEP clusters suggest that 1-AT has H-bond interactions with the ions ($[NO_3]^-$ and $[EA]^+$) and form a "bulky" ion. The average KBOs of the H-bond between 1-AT and $[EA]^+$ indicates stronger H-bonding interactions than the H-bond between 1-AT and $[NO_3]^-$. The H-bond interaction between 1-AT and $[EA]^+$ can be viewed as the formation of a "bulky" asymmetric cation. The formation of the bulky cation via H-bonds is essential because the bulky cations can lower the lattice energy and contribute to the eutectic character of the DeEP. [10,13,14,15]

Acknowledgement

The authors acknowledge Dr. Buu Pham and Dr. Dipayan Datta for discussions about applying RI-MP2 and RI-CCSD(T) methods to ionic liquids and deep eutectic solvents. The authors thank Dr. George Schoendorff, Dr. Jorge Galvez Vallejo and Mr. Daniel Del Angel for insightful discussions of the QUAO analysis for the H-bonded systems. Support for this work was provided by a grant from the Air Force Office of Scientific Research, under contract AFOSR FA9550-18-1-0321. This work was supported in part by high-performance computer time and resources from the DoD High Performance Computing Modernization Program.

Reference:

1. D. R. MacFarlane, M. Forsyth, E. I. Izgorodina, A. P. Abbott, G. Annat and K. Fraser, *Phys. Chem. Chem. Phys.*, 2009, **11**, 4962.
2. K. J. Fraser, E. I. Izgorodina, M. Forsyth, J. L. Scotta and D. R. MacFarlane, *Chem. Commun.*, 2007, 3817.
3. D. R. MacFarlane, N. Tachikawa, M. Forsyth, J.M. Pringle, P. C. Howlett, G.D. Elliot, G. D. J.H.J. Davis, M. Watanabe, P. Simon and C.A. Angell, Energy Applications of Ionic Liquids. *Energy Environ. Sci.* 2014, ***7***, 232.
4. J.A. Conrad, S. Kim and M.S. Gordon, Ionic liquids from a fragmented perspective. *Phys Chem. Chem. Phys.* 2019, **21**, 16878.
5. M. J. Earle and K. R. Seddon, *Pure Appl. Chem.*, 2000, **72**, 1391.
6. M. J. Earle, J. M. S. S. Esperanc, M. A. Gilea, J. N. C. Lopes, L. P. N. Rebelo, J. W. Magee, K. R. Seddon and J. A. Widegren, *Nature*, 2006, **439**, 831.
7. N. V. Plechkova and K. R. Seddon, *Chem. Soc. Rev.*, 2008, **37**, 123.
8. E. Bodo, A. Sferrazza, R. Caminiti, S. Mangialardo and P. Postorino, *J. Chem. Phys.*, 2013, **139**, 144309.
9. J.L. Anderson and K.D. Clark, Ionic liquids as tunable materials in (bio)analytical chemistry. *Anal.Bioanal. Chem.* 2018, **410**, 4565
10. E. L. Smith, A. P. Abbott and K. S. Ryder, *Chem. Rev.*, 2014, **114**, 11060.
11. A. A. Shamsuri, *Makara Journal of Science*, 2011.
12. R.J. Bernot, M.A. Brueseke, M.A. Evans-White and G.A. Lamberti, Acute and chronic toxicity of imidazolium-based ionic liquids on Daphnia magna. *Environ. Toxicol. Chem.* 2005, **24**, 87
13. B. B. Hansen, S. Spittle, B. Chen, D. Poe, Y. Zhang, J. M. Klein, A. Horton, L. Adhikari, T. Zelovich, B. W. Doherty, B. Gurkan, E. J. Maginn, A. Ragauskas, M. Dadmun, T. A. Zawodzinski, G. A. Baker, M. E. Tuckerman, R. F. Savinell and J. R. Sangoro, *Chemical Reviews*, 2021, **121**, 1232-1285.
14. Y. Dai, J. van Spronsen, G. J. Witkamp, R. Verpoorte and Y. H. Choi, *Anal. Chim. Acta*, 2013, **766**, 61.
15. G. Garcia, M. Atilhan and S. Aparicio, *J. Mol. Liq.*, 2015, **211**, 506.
16. A. P. Abbott, G. Capper, K. J. McKenzie and K. S. Ryder, *J. Electroanal. Chem.*, 2007, **599**, 288.
17. A. P. Abbott, K. J. Edler and A. J. Page, *The Journal of Chemical Physics*, 2021, **155**, 150401.
18. O. S. Hammond, H. Li, C. Westermann, A. Y. M. Al-Murshedi, F. Endres, A. P. Abbott, G. G. Warr, K. J. Edler and R. Atkin, *Nanoscale Horizons*, 2019, **4**, 158.
19. A. P. Abbott, P. M. Cullis, M. J. Gibson, R. C. Harris and E. Raven, *Green Chem.*, 2007, **9**, 868.
20. Y. Dai, G. J. Witkamp, R. Verpoorte, Y. H. Choi, Tailoring Properties of Natural Deep Eutectic Solvents with Water to Facilitate Their Applications. *Food Chem.* 2015, **187**, 14.
21. Y. Zhang, X. Lu, X. Feng, X. Y. Shi and X. Ji, Properties and applications of choline-based deep eutectic solvents. *Prog. Chem.* 2013, **25**, 881.
22. A. Paiva, R. Craveiro, I. Aroso, M. Martins, R. L. Reis and A. R. C. Duarte, *ACS Sustainable Chem. Eng.*, 2014, **2**, 1063.
23. L. Luo and N. Le Pierrès, in *Solar Energy Storage*, ed. B. Sørensen, Academic Press, Boston, 2015, pp. 27-62.

24. S. Tang, M. Zhang and M. Guo, A Novel Deep-Eutectic Solvent with Strong Coordination Ability and Low Viscosity for Efficient Extraction of Valuable Metals from Spent Lithium-Ion Batteries. *ACS ACS Sustainable Chem. Eng.* 2022, **10**, 975
25. Y. Ahmed, A. Quintana, G. Warmoth, S. Deplazes, A. Brand, J. Mills and S. Schneider, Solid+Solid=Liquid: An ON-Switch for Sensitivity in Deep Eutectic Solvents? *Propell. Explos. Pyroteh.* 2019, **44,** 1129
26. F. S. Mjalli and O. U. Ahmed, *Asia-Pac. J. Chem. Eng.*, 2016, **11**, 549.
27. T. Altamash, M. Atilhan, A. Aliyan, R. Ullah, G. García and S. Aparicio, *RSC Adv.*, 2016, **6**, 109201.
28. T. Jiao, H. Wang, F. Dai, C. Li and S. Zhang, *Ind. Eng. Chem. Res.*, 2016, **55**, 8848.
29. Q.-H. Lin, Y.-C. Li, Y.-Y. Li, Z. Wang, W. Liu, C. Qi and S.-P. Pang, *Journal of Materials Chemistry*, 2012, **22**, 666-674.
30. J.M. Guevara-Vela, E. Romero-Montalvo, V.A. Mora Gómez, R. Chávez-Calvillo, M. García-Revilla, E. Francisco, Á. M. Pendás and T. Rocha-Rinza, Hydrogen bond cooperativity and anticooperativity within the water hexamer. *Phys Chem Chem Phys* 2016, **18**, 19557-19566, 10.1039/C6CP00763E. DOI: 10.1039/C6CP00763E.
31. T. Steiner, The Hydrogen Bond in the Solid State. *Angew. Chem., Int. Ed.* 2002, **41**, 48-76
32. C. Pérez, M. T. Muckle, D. P. Zaleski, N. A. Seifert, B. Temelso, G. C. Shields, Z. Kisiel and B. H. Pate, *Science*, 2012, **336**, 897.
33. J. L. Galvez Vallejo, J. D. Heredia and M. S. Gordon, *Physical Chemistry Chemical Physics*, 2021, **23**, 18734-18743.
34. O. Mó, M. Yáñez and J. Elguero, *J. Chem. Phys.*, 1992, **97**, 6628.
35. K. Dong, S. Zhang and J. Wang, Understanding the Hydrogen Bonds in Ionic Liquids and Their Roles in Properties and Reactions. *Chem. Commun.* 2016, **52**, 6744.
36. A. Knorr and R. Ludwig, *Scientific Reports*, 2015, **5**, 17505.
37. K. Shiota, Y.-I. Izato, H. Matsunaga, H. Habu and A. Miyake, *Transactions of The Japan Society for Aeronautical and Space Sciences, Aerospace Technology Japan*, 2018, **16**, 93-97.
38. F. Weinhold and C. R. Landis, *Discovering Chemistry with Natural Bond Orbitals*; 2012.
39. J.P. Foster and F. Weinhold, Natural hybrid orbitals. *J. Am. Chem. Soc.* 1980, **102**, 7211
40. F. Weinhold and C.R. Landis, *Valency and bonding: a natural bond orbital donor-acceptor perspective*; Cambridge University Press, 2005.
41. E. D. Glendening, J. K. Badenhoop, A. E. Reed, J. E. Carpenter, J. A. Bohmann, C. M. Morales, C. R. Landis and F. Weinhold, *NBO 6.0*, 2013.
42. A.E. Reed, L.A. Curtiss and F. Weinhold. *Chem. Rev* 1988, **88**, 899.
43. S. J. Grabowski, *Chem. Rev.*, 2011, **111**, 2597.
44. E. Arunan, G. R. Desiraju, R. A. Klein, J. Sadlej, S. Scheiner, I. Alkorta, D. C. Clary, R. H. Crabtree, J. J. Dannenberg and P. Hobza, *Pure Appl. Chem.*, 2011, **83**, 1619.
45. A. J. Stone, *The Theory of Intermolecular Forces*; Oxford University Press 2013.
46. A. J. Stone, Computation of charge-transfer energies by perturbation theory. *Chem. Phys. Lett.* 1993, **211**, 101.
47. P. A. Hunt, C. R. Ashworth and R. P. Matthews, *Chemical Society Reviews*, 2015, **44**, 1257-1288.
48. I. Rozas, I. Alkorta and J. Elguero, *J. Phys. Chem. A*, 1999, **103**, 8861-8869.

49. M.S. Gordon, L. Slipchenko, H. Li and J.H. Jensen, The Effective Fragment Potential: A General Method for Predicting Intermolecular Interactions. *Annu. Rep. Comput. Chem.* 2007, **3**, 177.
50. M.S. Gordon, Q.A. Smith, P. Xu and L.V. Slipchenko, *Annu. Rev. Phys. Chem.* 2013, **64**, 553.
51. L. V. Slipchenko and P. K. Gurunathan, *Fragmentation: Toward Accurate Calculations on Complex Molecular Systems*, 2017, 183-208.
52. P. N. Day, J. H. Jensen, M. S. Gordon, S. P. Webb, W. J. Stevens, W. J., M. Krauss, D. Garmer, H. Basch and D. Cohen, *J. Chem. Phys.* 1996, **105**, 1968.
53. P. Xu and M. S. Gordon, Charge transfer interaction using quasiatomic minimal-basis orbitals in the effective fragment potential method. *J. Chem. Phys.* 2013, **139**, 11, Article. DOI: 10.1063/1.4829509.
54. H. Li, M. S. Gordon and J. H. Jensen, Charge transfer interaction in the effective fragment potential method. *J. Chem. Phys.* 2006, **124**, 16, Article. DOI: 10.1063/1.2196884.
55. A. J. Stone and A. J. Misquitta, Charge transfer in symmetry-adapted perturbation theory. *Chem. Phys. Lett.* 2009, **473**, 201.
56. B. T. Nebgen, H. D. Magurudeniya, K. W. C. Kwock, B. S. Ringstrand, T. Ahmed, S. Seifert, J.-X. Zhu, S. Tretiak and M. A. Firestone, *Faraday Discussions*, 2018, **206**, 159-181.
57. M. S. Gordon, J. M. Mullin, S. R. Pruitt, L. B. Roskop, L. V. Slipchenko and J. A. Boatz, Accurate Methods for Large Molecular Systems. *J. Phys. Chem. B* 2009, **113** 9646
58. B. Jeziorski, R. Moszynski, K. Szalewicz, Perturbation Theory Approach to Intermolecular Potential Energy Surfaces of van der Waals Complexes. *Chem. Rev.* 1994, **94**, 1887.
59. A. C. West, M. W. Schmidt, M. S. Gordon and K. A. Ruedenberg, Comprehensive analysis of molecule intrinsic quasi-atomic, bonding, and correlating orbitals. I. Hartree-Fock wave functions. *J. Chem. Phys.* 2013, **139**, 234107
60. A. C. West, J. J. Duchimaza Heredia, M. S. Gordon and K. Ruedenberg, *J. Phys. Chem. A*, 2017, **121**, 8884.
61. A. C. West, M. W. Schmidt, M. S. Gordon and K. Ruedenberg, Intrinsic resolution of molecular electronic wave functions and energies in terms of quasi-atoms and their interactions. *J. Phys. Chem. A* 2017, **121**, 1086.
62. W.C. Lu, C. Z. Wang, M. W. Schmidt, L. Bytautas, K. M. Ho and K. Ruedenberg, Molecule intrinsic minimal basis sets. I. Exact resolution of ab initio optimized molecular orbitals in terms of deformed atomic minimal-basis orbitals. *J. Chem. Phys.* 2004, **120**, 2629
63. A.C. West, M. W. Schmidt, M. S. Gordon and K. Ruedenberg. A Comprehensive Analysis in Terms of Molecule-Intrinsic, Quasi-Atomic Orbitals. III. The Covalent Bonding Structure of Urea. *J. Phys. Chem. A* 2015, **119** 10368
64. A. C. West, M. W. Schmidt, M. S. Gordon and K. Ruedenberg, A Comprehensive Analysis of Molecule-Intrinsic Quasi-Atomic Orbitals. IV. Bond Breaking and Bond Forming along the Dissociative Reaction Path of Dioxetane. *J. Phys. Chem. A* 2015, **119**, 10376.
65. G. Schoendorff, K. Ruedenberg and M. S. Gordon, *J. Phys. Chem. A,* 2021, **125**, 4836-4846.

66. J. J. Duchimaza Heredia, K. Ruedenberg, M. S. Gordon, M. S. Quasi-Atomic Bonding Analysis of Xe-Containing Compounds. *J. Phys. Chem. A* 2018, **122**, 3442.
67. J. J. Duchimaza Heredia, A. D. Sadow, M. S. Gordon, A Quasi-Atomic Analysis of Three-Center Two-Electron Zr–H–Si Interactions. *J. Phys. Chem. A* 2018, **122**, 9653.
68. G. Schoendorff, M. W. Schmidt, K. Ruedenberg and M. S. Gordon, *J. Phys. Chem. A*, 2019, **123**, 5249.
69. Q. Zhang and J. n. M. Shreeve, Ionic Liquid Propellants: Future Fuels for Space Propulsion. *Eur. J. Chem.* 2013, **19**, 15446
70. Q. Zhang and J. n. M. Shreeve. Energetic Ionic Liquids as Explosives and Propellant Fuels: A New Journey of Ionic Liquid Chemistry. *Chem. Rev.* 2014, **114**, 10527
71. N. A. Mehta and D. A. Levin, *Aerospace*, 2018, **5**, 1.
72. E. Sebastiao, C. Cook, A. Hu and M. Murugesu, *J. Mater. Chem. A*, 2014, **2**, 8153.
73. M. J. Wainwright, J. Rovey, S. Miller and B. D. Prince, 2019.
74. Y. Li, C. Oommen and S. M. Sarathy, *Propellants, Explosives, Pyrotechnics*, 2020, **45**, 1949-1958.
75. P. K. Gurunathan, A. Acharya, D. Ghosh, D. Kosenkov, I. Kaliman, Y. Shao, A. I. Krylov and L. V. Slipchenko, *The Journal of Physical Chemistry B*, 2016, **120**, 6562
76. M. Krauss, Effective fragment potentials and spectroscopy at enzyme active sites. *Comput. Chem. (Oxford, U. K.)* 1995, **19**, 33.
77. Y. L. Kim, Y. Han, J. W. Evans and M. S. Gordon, Effective Fragment Potential-Based Molecular Dynamics Studies of Diffusion in Acetone and Hexane. *J. Phys. Chem. A* 2021, **125**, 3398.
78. Y. L. Kim, M. S. Gordon, A. Garcia and J. W. Evans, Rotational and translational diffusion of liquid n-hexane: EFP-based molecular dynamics analysis. *J. Chem. Phys.* 2022, **156**, 114503.
79. S. Y. S. Tan and E. I. Izgorodina, Comparison of the Effective Fragment Potential Method with Symmetry-Adapted Perturbation Theory in the Calculation of Intermolecular Energies for Ionic Liquids. *J. Chem. Theory Comput.* 2016, **12**, 2553
80. D. D. Kemp, J. M. Rintelman, M. S. Gordon and J. H. Jensen, *Theor. Chem. Acc.*, 2010, **125**, 481.
81. A.C. West, M. W. Schmidt, M. S. Gordon and K. Ruedenberg. A Comprehensive Analysis of Molecule-Intrinsic Quasi-Atomic Orbitals. II. Strongly Correlated MCSCF Wave Functions. *J. Phys. Chem. A* 2015, **119**, 10360.
82. M. Katouda and S. Nagase, *Int. J. Quantum Chem.*, 2009, **109**, 2121.
83. B. Q. Pham and M. S. Gordon, *J. Chem. Theory Comput.*, 2019, **15**, 2254.
84. T. Y. Takeshita, W. A. de Jong, D. Neuhauser, R. Baer and E. Rabani, *J. Chem. Theory Comput.*, 2017, **13**, 4605.
85. F. Weigend, M. Häser, H. Patzelt and R. Ahlrichs, RI-MP2: Optimized Auxiliary Basis Sets and Demonstration of Efficiency. *Chem. Phys. Lett.* 1998, **294**, 143.
86. F. Weigend and M. Häser., RI-MP2: first derivatives and global consistency. *Theor. Chem. Acc.* 1997, **97,** 331
87. D. Datta and M. S. Gordon, *Journal of Chemical Theory and Computation*, 2021, **17**, 4799-4822.
88. B. Q. Pham and M. S. Gordon, *J. Chem. Theory Comput.*, 2019, **15**, 5252.
89. M.W. Schmidt, K. K. Baldridge, J. A. Boatz, S. T. Elbert, M. S. Gordon, J. H. Jensen, S. Koseki, N. Matsunaga, K. A. Nguyen, S. J. Su, et al. GENERAL ATOMIC AND

MOLECULAR ELECTRONIC-STRUCTURE SYSTEM. *J. Comput. Chem.* 1993, **14**, 1347

90. M. S. Gordon and M. W. Schmidt, Advances in electronic structure theory: GAMESS a decade later. *Theory and Applications of Computational Chemistry: the First Forty Years* 2005, 1167-1189.
91. G. M. J. Barca, C. Bertoni, L. Carrington, D. Datta, N. De Silva, J. E. Deustua, D. G. Fedorov, J. R. Gour, A. O. Gunina and E. Guidez, *J. Chem. Phys.*, 2020, **152**, 154102.
92. B. M. Bode and M. S. Gordon, *J. Mol. Graphics Modell.*, 1998, **16**, 133.
93. W. A. Henderson, P. Fylstra, H. C. De Long, P. C. Trulove and S. Parsons, *Physical Chemistry Chemical Physics*, 2012, **14**, 16041.
94. G. Kaplan, G. Drake, K. Tollison, L. Hall and T. Hawkins, Synthesis, characterization, and structural investigations of 1-amino-3-substituted-1,2,3-triazolium salts, and a new route to 1-substituted-1,2,3-triazoles. *J. Heterocycl. Chem.* 2005, **42**, 19
95. E. Bodo, S. Mangialardo, F. Ramondo, F. Ceccacci and P. Postorino, *J. Phys. Chem. B*, 2012, **116**, 13878.
96. P. N. Day, R. Pachter, M. S. Gordon and G. N. Merrill, A study of water clusters using the effective fragment potential and Monte Carlo simulated annealing. *J. Chem. Phys.* 2000, **112**, 2063.
97. P. Jurecka, J. Sponer, J. Cerny and P. Hobza, Benchmark database of accurate (MP2 and CCSD(T) complete basis set limit) interaction energies of small model complexes, DNA base pairs, and amino acid pairs. *Phys.Chem. Chem. Phys.* 2006, **8**, 1985
98. J. Řezáč, P. Jurečka, K. E. Riley, J. Černý, H. Valdes, K. Pluháčková, K. Berka, T. Řezáč, M. Pitonák and J. Vondrášek, Quantum Chemical Benchmark Energy and Geometry Database for Molecular Clusters and Complex Molecular Systems (www.begdb.com): A Users Manual and Examples. *Collect. Czech. Chem. Commun.* 2008, **73**, 1261.
99. D. Ghosh, D. Kosenkov, V. Vanovschi, C. F. Williams, J. M. Herbert, M. S. Gordon, M. W. Schmidt, L. V. Slipchenko and A. I. Krylov, Noncovalent Interactions in Extended Systems Described by the Effective Fragment Potential Method: Theory and Application to Nucleobase Oligomers. *J. Phys. Chem. A* 2010, **114**, 12739.
100. J. C. Flick, D. Kosenkov, E. G. Hohenstein, C. D. Sherrill and L. V. Slipchenko, Accurate Prediction of Noncovalent Interaction Energies with the Effective Fragment Potential Method: Comparison of Energy Components to Symmetry-Adapted Perturbation Theory for the S22 Test Set. *J. Chem. Theor. Comp.* 2012, **8**, 2835
101. N. Dubinets and L. V. Slipchenko, *The Journal of Physical Chemistry A*, 2017, **121**, 5301-5312.
102. G. N. Simm, J. Proppe and M. Reiher, *CHIMIA*, 2017, **71**, 202.
103. M. S. Gordon, E. Maginn and R. Rogers, *Synthesis, Characterization and Simulation of Ionic Liquids*; Iowa State University Ames United States, 2018.
104. P. A. Hunt, K. Kirchner and T. Welton, Characterising the Electronic Structure of Ionic Liquids: An Examination of the 1-Butyl-3-Methylimidazolium Chloride Ion Pair. *Eur. J. Chem.* 2006, **12** 6762
105. E. I. Izgorodina, D. R and MacFarlane, Nature of Hydrogen Bonding in Charged Hydrogen-Bonded Complexes and Imidazolium-Based Ionic Liquids. *J. Phys. Chem. B* 2011, **115**, 14659
106. E. I. Izgorodina, Z. L. Seeger, D. L. A. Scarborough and S. Y. S. Tan, *Chem. Rev.*, 2017.

107. B. Kirchner, O. Hollóczki, J. N. Canongia Lopes and A. A. H. Pádua, *Wiley Interdiscip. Rev.: Comput. Mol. Sci.*, 2014, **5**, 202.
108. B. Kirchner, J. Hutter, I. Kuo and C. Mundy, *Int. J. Mod. Phys. B*, 2004, **18**, 1951.
109. S. Tsuzuki, H. Tokuda, K. Hayamizu and M. Watanabe, *J. Phys. Chem. B,* 2005, **109**, 16474.
110. S. Tsuzuki and H. P. Luthi, Interaction energies of van der Waals and hydrogen bonded systems calculated using density functional theory: Assessing the PW91 model. *J. Phys. Chem.* 2001, **114**, 3949
111. M. Addicoat, R. Atkin, J. N. Canongia Lopes, M. Costa Gomes, M. Firestone, R. Gardas, S. Halstead, C. Hardacre, L. J. Hardwick, J. Holbrey, P. Hunt, V. Ivaništšev, J. Jacquemin, R. Jones, B. Kirchner, R. Lynden-Bell, D. Macfarlane, G. Marlair, H. Medhi, M. Mezger, A. Pádua, I. Pantenburg, S. Perkin, J. E. S. J. Reid, M. Rutland, S. Saha, K. Shimizu, J. M. Slattery, M. Swadźba-Kwaśny, S. Tiwari, S. Tsuzuki, B. Uralcan, A. Van Den Bruinhorst, M. Watanabe and J. Wishart, *Faraday Discussions*, 2018, **206**, 291.
112. R. Hayes, S. Imberti, G. G. Warr and R. Atkin, *Angew. Chem., Int. Ed.*, 2013, **52**, 4623.
113. S. Koßmann, J. Thar, B. Kirchner, P. A. Hunt and T. Welton, *J. Chem. Phys.*, 2006, **124**, 174506.
114. A. A. H. Pádua, M. F. C. Gomes and J. N. A. C. Lopes, *Acc. Chem. Res.*, 2007, **40**, 1087.
115. I. Konovalova, Y. Nelyubina, K. A. Lyssenko, B. V. Paponov and O. V. Shishkin, *J. Phys. Chem. A* 2011 **115**, 8550
116. E. Thomas, K. P. Vijayalakshmi and B. K. George, in *Theoretical and Computational Approaches to Predicting Ionic Liquid Properties*, eds. A. Joseph and S. Mathew, Elsevier, 2021, pp. 69-86.
117. A. Rivera-Pousa, J. M. Otero-Mato, A. Coronas, A. J. Stone, R. M. Lynden-Bell, T. Méndez-Morales and L. M. Varela, *Journal of Molecular Liquids*, 2020, **320**, 114437.
118. K. Low, S. Y. S. Tan and E. I. Izgorodina, An ab initio Study of the Structure and Energetics of Hydrogen Bonding in Ionic Liquids. *Front. Chem.* 2019, **7**, Original Research.
119. S. S. Xantheas, Cooperativity and hydrogen bonding network in water clusters. *Chem. Phys.* 2000, **258**, 225.
120. J. D. Cruzan, L. B. Braly, K. Liu, M. G. Brown, J. G. Loeser and R. J. Saykally, *Science*, 1996, **271**, 59-62.
121. C. Peschel, C. Dreßler and D. Sebastiani, *Molecules*, 2020, **25**, 5722.
122. G. Gilli and P. Gilli, *The Nature of the Hydrogen Bond: Outline of a Comprehensive Hydrogen Bond Theory*, OUP Oxford, 2009.
123. U. B. Patil, A. S. Singh and J. M. Nagarkar, *RSC Adv.*, 2014, **4**, 1102.
124. G. C. Pimentel, *J. Chem. Phys.*, 1951, **19**, 446.
125. R. E. Rundle, *Rec. Chem. Prog*, 1962, **23**, 194.
126. C. T. Nemes, C. J. Laconsay and J. M. Galbraith, *Physical Chemistry Chemical Physics*, 2018, **20**, 20963.
127. M. S. Gordon, M. T. Carroll, J. H. Jensen, L. P. Davis, L. W. Burggraf and M. Guidry, *Organometallics*, 1991, **10**, 2657.